https://doi.org/10.5194/egusphere-2024-360
Preprint. Discussion started: 8 February 2024

In-plume and out-of-plume analysis of aerosol-cloud interactions derived from the 2014-15 Holuhraun volcanic eruption

Amy H. Peace[1,3], Ying Chen[2], George Jordan[3], Daniel G. Partridge[1], Florent Malavelle[3], Eliza Duncan[1], and Jim M. Haywood[1,3]

[1]Faculty of Environment, Science and Economy, University of Exeter, Exeter, EX4 4QE, UK
[2]School of Geography, Earth and Environmental Sciences, University of Birmingham, Birmingham, B15 2TT, UK
[3]Met Office, Exeter, EX1 3PB, UK

Correspondence to: Amy H. Peace (amy.h.peace@metoffice.gov.uk)

Abstract. Aerosol effective radiative forcing (ERF) has persisted as the most uncertain aspect of anthropogenic forcing over the industrial period, limiting our ability to constrain estimates of climate sensitivity and to confidently predict 21st century climate change. Aerosol-cloud interactions are the most uncertain component of aerosol ERF. The 2014-15 Holuhraun volcanic eruption acted as large source of sulphur dioxide, providing an opportunistic experiment for studying aerosol-cloud interactions at a climatically relevant scale. We evaluate the observed aerosol-induced perturbation to cloud properties inside the volcanic plume in the first month of the eruption and compare the results to those from UKESM1 (UK Earth System Model). In the first two weeks, as expected, we find an in-plume shift to smaller and more numerous cloud droplets in both the observations and the simulations, as well as an observed change in the distribution of liquid water path (LWP) values inside the plume. However, in the third week, the in-plume shift to smaller and more numerous cloud droplets is neither observed nor modelled, and there are discrepancies between the observed and modelled response in the fourth week. Analysis of the model simulations and trajectory modelling reveals that airmass history and background meteorological factors can strongly influence aerosol-cloud interactions between the weeks of our analysis. Overall, our study supports the findings of many previous studies; that the aerosol impact on cloud effective radius is significant, with a less significant effect on in-cloud LWP.

https://doi.org/10.5194/egusphere-2024-360
Preprint. Discussion started: 8 February 2024

1 Introduction

The evolution of aerosol emissions is thought to have profoundly impacted climate over the industrial period. Increasing emissions of anthropogenic aerosols and their gaseous precursors has exerted a negative radiative forcing on the climate system through the interaction of aerosols with clouds and radiation (Bellouin et al., 2020). The negative radiative forcing of aerosols has masked a proportion of warming from rising greenhouse gas emissions (Eyring et al., 2021), and led to large-scale changes in the water cycle and atmospheric circulation (Douville et al., 2021). Over the coming decades reductions in anthropogenic aerosol emissions are expected due to more ambitious climate change and air quality mitigation policies (Rao et al., 2017). Despite the importance of aerosol-climate interactions, aerosol radiative forcing is the most uncertain component of anthropogenic radiative forcing over the industrial period (Forster et al., 2021). The uncertainty in the magnitude of aerosol radiative forcing impacts the accuracy in which we can project near-term future climate changes (Andreae et al., 2005; Seinfeld et al., 2016; Peace et al., 2020; Watson-Parris and Smith, 2022). Aerosol-cloud interactions (ACI) make up the largest component of the uncertainty in aerosol radiative forcing (Bellouin et al., 2020). It is therefore an important task to continue to improve our understanding of ACI to predict future climate change more confidently.

Marine low-level liquid clouds strongly reflect shortwave radiation. Only small changes in their properties can have a significant impact of the radiative balance of the Earth system (Wood, 2012). Understanding how aerosols modify the properties of these clouds has therefore been the focus of much research. Conceptually, aerosols modify the properties of clouds through a chain of events (e.g. Haywood and Boucher, 2000). Firstly, aerosols act as cloud condensation nuclei (CCN). An increase in aerosol leads to an increase in cloud droplet number concentrations (N_d), and for a constant amount of cloud water, a reduction in cloud droplet effective radius (r_{eff}). Smaller and more numerous cloud droplets increase the albedo of clouds (Twomey, 1974). These effects have been widely observed (e.g. Bréon et al., 2002; Feingold et al., 2003). An increase in N_d may initiate further adjustments to cloud properties, such as changes in liquid water path (LWP) and cloud fraction, although bidirectional responses in LWP to an increase in N_d have been observed (e.g. Toll et al., 2019) and simulated (e.g. Ackerman et al., 2004). The directionality of the LWP response likely depends on the meteorological conditions present and accordingly whether smaller cloud droplets lead to precipitation suppression which can potentially increase LWP (Albrecht, 1989; Pincus and Baker, 1994), or if the smaller droplets lead to enhanced evaporation and decreased sedimentation which can enhance entrainment and decrease LWP (Ackerman et al., 2004; Bretherton et al., 2007). Recent research has shown significant cancellation of the positive and negative LWP responses is likely at large scales resulting in a weak LWP response to increased aerosol globally (Toll et al., 2019). However, global climate models (GCMs) can disagree with evidence from observations and higher resolution models on the magnitude and sign of the LWP response to increased N_d (Toll et al., 2017; Gryspeerdt et al., 2019). The uncertain response of LWP to increased N_d demonstrates why cloud adjustments to an increase in N_d remain poorly constrained, despite being able to enhance or counteract an increase in cloud albedo due to an increase in smaller cloud droplets.

https://doi.org/10.5194/egusphere-2024-360
Preprint. Discussion started: 8 February 2024

'Opportunistic' experiments offer a way to improve our understanding of aerosol-cloud interactions in a system where both the aerosol-perturbed and unperturbed background cloud state are reasonably well established (Christensen et al., 2022). The magnitude and sign of ACI can depend on numerous factors including background aerosol concentrations, meteorology and cloud properties (e.g. Stevens and Feingold, 2009; Carslaw et al., 2013). Opportunistic experiments can therefore provide a way to isolate ACI in environments with similar conditions or provide insight into how background conditions affect ACI. Key opportunistic experiments that have been used to study ACI include ship tracks, industrial plumes, wildfires and volcanic eruptions (e.g. Malavelle et al., 2017; Toll et al., 2017; Christensen et al., 2022). In this study, we utilise the 2014-15 Holuhraun effusive volcanic eruption as an opportunistic experiment to assess and improve our understanding of ACI.

The 2014-15 Holuhraun eruption in Iceland (64.85°N, 16.83°W) began on 31st August 2014 and ended on 27th February 2015. This eruption was one of the largest sources of tropospheric volcanic emissions since the 1783-1784 Laki eruption (Ilyinskaya et al., 2017). Ground-based and satellite observations show that the Holuhraun eruption emitted large amounts of SO_2 (up to ~100 kt SO_2 day^{-1}) into the troposphere (Pfeffer et al., 2018; Carboni et al., 2019). The daily SO_2 emitted from the eruption was at least a factor of 3 larger than anthropogenic emissions from the whole of Europe (Schmidt et al., 2015). Once emitted, SO_2 is readily oxidised into sulphate aerosol, therefore, the Holuhraun eruption created a large aerosol plume. As a result, the 2014-15 Holuhraun eruption provides an opportunistic experiment to investigate ACI hypotheses at a large, climatically relevant scale.

A handful of studies have leveraged the Holuhraun eruption to study ACI using differing approaches. Malavelle et al., (2017) used a climatological approach to identify aerosol-cloud interactions following the eruption. Their results showed a decrease in r_{eff} during October 2014 in both satellite observations and climate model simulations compared to the climatological mean. Yet, satellite observations revealed no clear perturbation to LWP or cloud fraction, unlike climate model responses showing varying LWP changes. Chen et al., (2022) used a machine learning approach to predict the cloud properties that would be expected for September and October 2014 without the presence of the volcanic eruption, given the meteorological conditions. The predicted cloud properties were then compared to satellite observations to isolate the aerosol perturbation to cloud properties following the eruption. Similarly to the climatological approach of Malavelle et al. 2017, the machine learning approach isolated a decrease in r_{eff} but no detectable change in LWP. However, the machine learning approach revealed an aerosol-induced increase in cloud fraction. Lastly, Haghighatnasab et al., (2022) focused on the first week following the eruption, comparing cloud properties inside and outside the SO_2 eruption plume in satellite observations and a high-resolution model. This plume analysis approach showed an increase in N_d and decrease in r_{eff} inside the eruption plume in line with the results from Malavelle et al. (2017) and Chen et al., (2022). However, Haghighatnasab et al., (2022) show an observed shift in the distribution of in-plume LWP values, with decreased likelihood of low LWP values to and increased likelihood of higher LWP values, which is further exaggerated in the high-resolution model.

https://doi.org/10.5194/egusphere-2024-360
Preprint. Discussion started: 8 February 2024

Our study builds on these previous analyses of aerosol-cloud interactions derived following the 2014-15 Holuhraun eruption. We use satellite observations of aerosol and cloud properties to evaluate the observed ACI following the volcanic eruption and compare our results to simulations from UKESM1 (UK Earth System Model). We add to the plume analysis approach utilised in Haghighatnasab et al., (2022) by using a more detailed plume masking method that excludes pixels which are not likely to be near the plume and hence unlikely to be representative of the cloud fields being perturbed. We also extend the plume analysis from the first week of September 2014 that was analysed in Haghighatnasab et al., (2022) to the rest of the month. The longer time period allows us to investigate how airmass history and background meteorological factors influence aerosol-cloud interactions between the weeks of our analysis using the HYSPLIT trajectory model (The Hybrid Single-Particle Lagrangian Integrated Trajectory model).

2 Data and methods

2.1 Defining a plume mask from satellite observation of SO_2

We use the column amount of SO_2 in the lower troposphere to define a plume mask that is used to compare cloud properties inside and outside of the aerosol plume following the eruption.

We obtain the SO_2 data product from the Ozone Mapping and Profiler Suite (OMPS) Nadir Mapper (NM) onboard the NASA-NOAA Suomi National Polar-orbiting partnership (SNPP) satellite that was launched in October 2011 (Flynn et al., 2014; Seftor et al., 2014). The Nadir Mapper is a UV spectrometer that measures backscattered solar UV radiance from the Earth and solar irradiance. SO_2 absorbs strongly in the UV and therefore the vertical column density of SO_2 can be retrieved from satellite measurements of the UV spectrum. The column amount of SO_2 is retrieved from OMPS using a principal component analysis (PCA) algorithm (Li et al., 2017, 2020b). We use V2.0 of the SO_2 data product in our analysis (NMSO2_PCA_L2 V2.0) (Li et al., 2020a).

The PCA algorithm provides six estimates of the total SO_2 vertical column density based on a priori profiles of the centre of mass altitude (Li et al., 2020a). We use the data product that is based on an SO_2 plume height in the lower troposphere (TRL) at 3 km, which is a typical height of volcanic degassing and moderate eruptions. Carboni et al., (2019) showed the altitude of the centre of mass of the SO_2 Holuhraun eruption plume was mainly confined to within 0-6 km. Following the OMPS quality control procedure, pixels near the edge of the swath and where the solar zenith angle (SZA) > 70° are excluded. OMPS has a nadir resolution of 50 x 50 km and crosses the equator about 13:30 local time. We resample swath data to a regular grid with resolution of 0.5 x 0.5° using a nearest neighbour method. When creating the plume mask for use with the model simulations, we first re-grid the 0.5 x 0.5° OMPS data to the same resolution as the model simulations. We apply the following analysis in a "Holuhraun" domain of longitude 45°W to 30°E and latitude of 45°N to 80°N (e.g. as in Figure 1).

https://doi.org/10.5194/egusphere-2024-360
Preprint. Discussion started: 8 February 2024

After processing the SO_2 data product to gridded data, the next step in our analysis is to define a suitable plume mask and bounding region around the plume to use in isolating in-plume versus out-of-plume cloud properties. We use a threshold exceedance and filtering approach to define the eruption plume mask. Firstly, we define grid cells where the total column amount of SO_2 > 1 DU as being in-plume. This masking approach and threshold exceedance choice was also used in Haghighatnasab et al., (2022). Next, we apply a 3 x 3-pixel median filter to reduce noise in the mask and minimise individual grid cells with SO_2 > 1 DU that are not likely to be part of the volcanic plume and would affect the bounding box region. Using the median filter, for every n x n pixels, the centre pixel is replaced by taking the median of the values inside the matrix. The median filter approach has previously been used to remove random classification errors when detecting methane plumes from point sources (Varon et al., 2018). Lastly, each day we define a bounding box around the plume as the minimum to maximum latitude and longitude of the plume extent. We use this bounding box approach rather than using the whole domain to minimise differences in meteorological conditions between inside and outside the plume, which can confound the aerosol effect on cloud properties (e.g. McCoy et al., 2020). An example of the plume mask and bounding region with and without the median filter is shown in Figure 1, and the daily column amount of SO_2 and bounding region is shown in the animation S1.

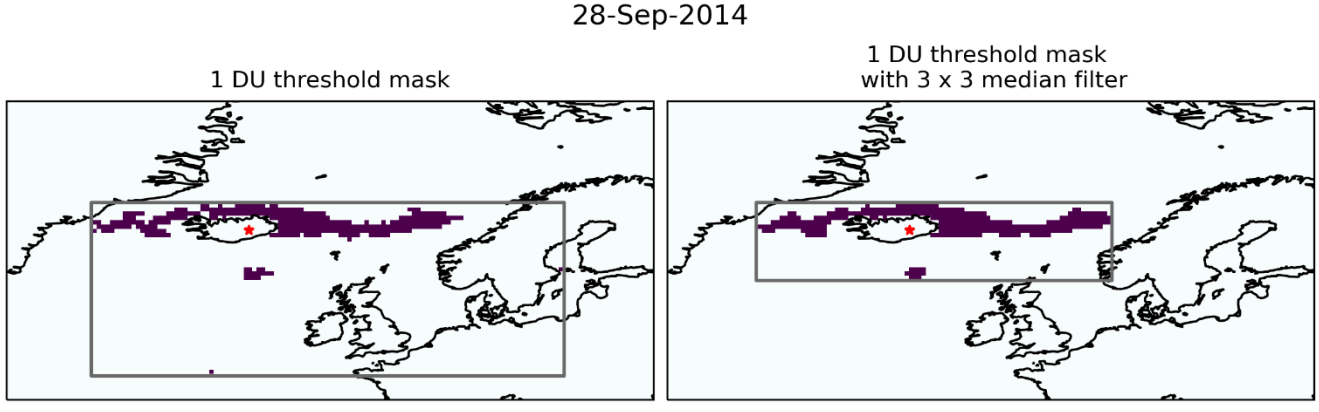

Figure 1: An example of the plume mask and bounding region on 28th Sep 2014 where total column amount of SO_2 > 1 DU without filtering (left) and with (right) a 3 x 3 median filter.

2.2 Satellite observations of cloud properties

We use Level 2 Collection 6.1 products of the MODerate resolution Imaging Spectroradiometer (MODIS) onboard the polar-orbiting Aqua satellite (Platnick et al, 2015; Platnick et al., 2017) to evaluate perturbations to cloud properties inside the SO_2 plume. We analyse liquid N_d, r_{eff}, cloud fraction and in-cloud LWP. In Level 2 MODIS products, r_{eff}, cloud water path and cloud optical thickness are retrieved from observed multispectral reflectances using a radiative transfer model at 1 km nadir resolution. Cloud phase is retrieved through the phase retrieval algorithm at 1 km resolution. Cloud fraction is retrieved at 5 km resolution by averaging the presence of cloud identified at pixel level (Platnick et al., 2017). We derive liquid N_d from liquid cloud r_{eff} and cloud optical thickness (τ_c) assuming an adiabatic cloud:

https://doi.org/10.5194/egusphere-2024-360
Preprint. Discussion started: 8 February 2024

$$N_d = \alpha \tau_c^{0.5} r_{eff}^{-2.5} \quad (1)$$

Where, α is 1.37 10^{-5} $m^{-0.5}$. Only data pixels where cloud optical thickness is between 4 and 70, and r_{eff} between 4 and 30 μm are retained where the retrieval is the most reliable (Quaas et al., 2006), but N_d derived in this way is still subject to uncertainties related to the cloud adiabaticity assumption and uncertainty in underlying cloud property retrievals (Gryspeerdt et al., 2022). We use cloud water path as a proxy for LWP which is a suitable assumption for non-raining liquid clouds (Zhou et al., 2016). We aggregate the Level 2 swath data to a 0.5 x 0.5-degree resolution grid for each day.

We examine differences in cloud properties inside vs outside the plume mask described in Section 2.1 for marine liquid cloud with cloud top heights between 1-5 km to better isolate where the aerosol plume interacts with liquid clouds. Satellite observations show the SO_2 plume centre of mass is within 0-6 km (Carboni et al., 2019; Jordan et al., 2023) and ground base observations show eruption plume top heights of 0.3-5.5 km (Pfeffer et al., 2018).

2.3 UKESM1 simulations

We compare the perturbation of in-plume cloud properties observed from MODIS to the atmosphere-only version of the UK Earth System Model (hereafter UKESM1-A) (Sellar et al., 2019; Mulcahy et al., 2020). We also use the UKESM1-A simulations to further investigate the influence of meteorology on aerosol-cloud interactions.

UKESM1 is the first version of the UK Earth System Model and contributed to the sixth Coupled Model Intercomparison Project (CMIP6) (Eyring et al., 2016; Sellar et al., 2019). UKESM1 is based on the HadGEM3-GC3.1 physical climate model (Kuhlbrodt et al., 2018; Williams et al., 2018) coupled to several earth system processes including interactive stratosphere-troposphere chemistry from the UK Chemistry and Aerosol model (UKCA) (Archibald et al., 2020). The aerosol scheme within UKCA is the modal version of the Global Model of Aerosol Processes (GLOMAP-mode) (Mann et al., 2010; Mulcahy et al., 2020). In the atmosphere-only version of UKESM1 (UKESM1-A), sea surface temperatures and sea ice concentrations are prescribed from Program for Climate Model Diagnosis and Intercomparison (Rayner et al., 2003). Vegetation and ocean biological fields are prescribed from a member of the UKESM1 CMIP6 historical ensemble (Sellar et al., 2019). The model resolution used is N96L85, which is a horizontal resolution of 1.875 x 1.25° at the equator, with 85 atmospheric levels.

In the Holuhraun eruption simulation of this UKESM1 setup, the volcanic SO_2 emissions are distributed equally between 0.8 km and 3 km in the grid cell containing the eruption vent following the magnitude and altitude profile of emissions (Malavelle et al., 2017). We refer to the simulation that includes volcanic emissions as UKESM1-Hol hereafter. A control simulation was also performed without the Holuhraun eruption emissions which we refer to as UKESM-Ctrl. The control simulations enable us to assess whether any of the differences in our model simulations are simply due to differences in the

https://doi.org/10.5194/egusphere-2024-360
Preprint. Discussion started: 8 February 2024

meteorology, rather than due to the aerosol perturbations. The eruption and control simulations include background aerosol emissions from anthropogenic and natural sources. The modelled horizontal winds and potential temperature between approximately 1.3 to 80 km are nudged towards ERA-Interim reanalysis on a 6-hourly time scale to reduce model internal variability. The model output fields are extracted at high temporal resolution (3 or 6-hourly output) for comparison to observational data. The spatial and chemical evolution of the Holuhraun aerosol pollution in these UKESM-A simulations has recently been evaluated in a multi-model comparison framework in Jordan et al. (2023).

To aid the comparison of modelled cloud properties with MODIS, we use the Cloud Feedback Model Intercomparison Project (COSP) MODIS simulator for model output where possible. COSP is a software tool that uses output from climate models to produce data comparable to that retrieved from several satellite instruments (Bodas-Salcedo et al., 2011). N_d was calculated from COSP output using the same calculation and filtering as for the MODIS data.

2.4 Trajectory modelling

The Hybrid Single Particle Lagrangian Trajectory (HYSPLIT4) model (Stein et al., 2015) was used to calculate 10-day back trajectories from the Holuhraun eruption vent. For consistency with UKESM1-A simulations, ERA-Interim 6-hourly reanalysis (Dee et al., 2011), re-gridded to 1.0° x 1.0° were used to drive HYSPLIT. For every hour during September 2014, a 27-member ensemble of 10-day backward trajectories was initiated from the eruption site (64.85°N, 16.83°W) at a starting altitude of 2000 m agl (above ground level). The 27-member ensemble was created to sample the uncertainty associated with location accuracy. The centre trajectory of the ensemble is initialised at the coordinates above, with the remaining 26 members offset by a fixed grid factor of 1.0° of latitude/longitude in the horizontal and 0.01 sigma units in the vertical, forming a 3-dimensional space with 27 trajectory initialisation points.

We create transport probability function maps to investigate the dominant movement path of the air masses during September 2014. The transport probability function, $P(A_{i,j})$, represents the probability (%) of a backward trajectory passing through a specific grid cell. $A_{i,j}$was calculated as:

$$A_{i,j} = \frac{n_{i,j}}{N} \quad (2)$$

Where $n_{i,j}$ corresponds to the number of distinct trajectory visits within a grid cell, and N corresponds to the total number of trajectories. The maps allow a qualitative assessment of whether the air-masses reaching Holuhraun are from geographic areas that are relatively pristine or influenced by anthropogenic emissions and also help characterise the thermodynamic properties of those air-masses.

https://doi.org/10.5194/egusphere-2024-360
Preprint. Discussion started: 8 February 2024

3 Results

3.1 Evolution of the Holuhraun SO_2 plume

Our analysis uses the plume masks derived from the observed column amount of SO_2 to isolate cloud properties inside versus outside the aerosol plume formed from the 2014-15 Holuhraun eruption (see section 2.1). Variability in meteorology and cloud state across a domain can make the impact of aerosol perturbations to cloud properties difficult to isolate, for example, if the aerosol influenced cloud fields experience different conditions than the unperturbed cloud fields e.g. (Christensen et al., 2022). Therefore, we define a bounding box area around our plume mask to minimise differences in meteorological conditions. Figure 2 shows a snapshot of the column amount of SO_2 within our plume mask and the corresponding bounding regions for the middle day in each of the four weeks in September 2014 that we analyse. Supplementary Figure S1 shows an animation of the plume mask and bounding region for all the days analysed.

On many of the days in September 2014, the observed SO_2 plume disperses to the north-east of the eruption site. There are a handful of days within the month when the plume was transported towards Western Europe where it triggered air pollution events (Ialongo et al., 2015; Schmidt et al., 2015; Boichu et al., 2016; Steensen et al., 2016; Twigg et al., 2016; Zerefos et al., 2017). Our plume masking and bounding box method appears to track the spatial evolution of the observed SO_2 plume well for most days in September. Figure 2 and supplementary Figure S2 show the daily mean total column amount of SO_2 for the UKESM1-Hol simulations, and the corresponding plume mask and bounding region if derived from the model simulations. In common with simulations of explosive volcanic eruptions that are nudged to ERA reanalyses (Haywood et al., 2010; Wells et al., 2023), the SO_2 plume simulated in the model agrees well with the spatial location of the SO_2 plume observed from OMPS which gives us confidence in using the SO_2 mask derived from observations to evaluate the model simulations. Jordan et al., (2023) also show that the UKESM1-Hol simulations accurately capture the evolution of the volcanic plume in September and October 2014 when compared SO_2 retrieved from the IASI (Infrared Atmospheric Sounding Interferometer) satellite instrument. The recommended quality control procedure for OMPS involves excluding pixels where the SZA > 70°. Due to the high latitude of the eruption, this procedure excludes pixels at the top of our domain as September progresses and would also exclude pixels from the MODIS dataset that are less reliable. The UKESM1-Hol plume mask and bounding region therefore has a further northward extent than the OMPS plume mask towards the end of September.

https://doi.org/10.5194/egusphere-2024-360
Preprint. Discussion started: 8 February 2024

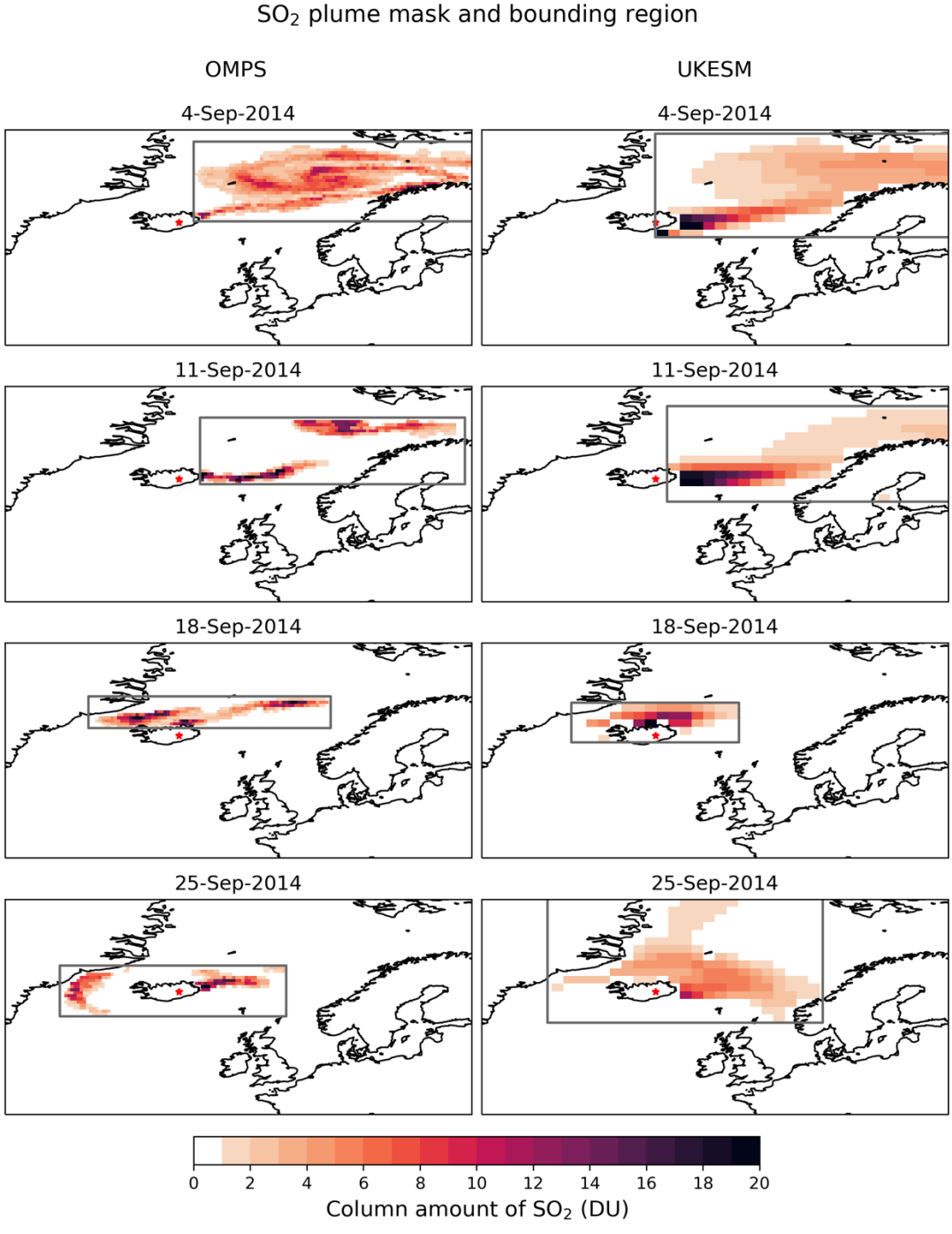

Figure 2: Total column amount of SO_2 (Dobson Units) retrieved from OMPS and simulated in UKESM1-Hol within the plume mask for the midweek day of the four weeks in September 2014 being analysed. The plume mask is defined where the total amount of SO_2 exceeds 1 DU. A 3 x 3 median filter is applied to the OMPS mask to reduce noise, as described in Section 2.1. We do not apply the mask to UKESM1-Hol due to the coarser data. The grey box shows the bounding box region surrounding the plume mask which we conduct our in-plume vs out-of-plume analysis within. The red star shows location of the eruption site.

https://doi.org/10.5194/egusphere-2024-360
Preprint. Discussion started: 8 February 2024

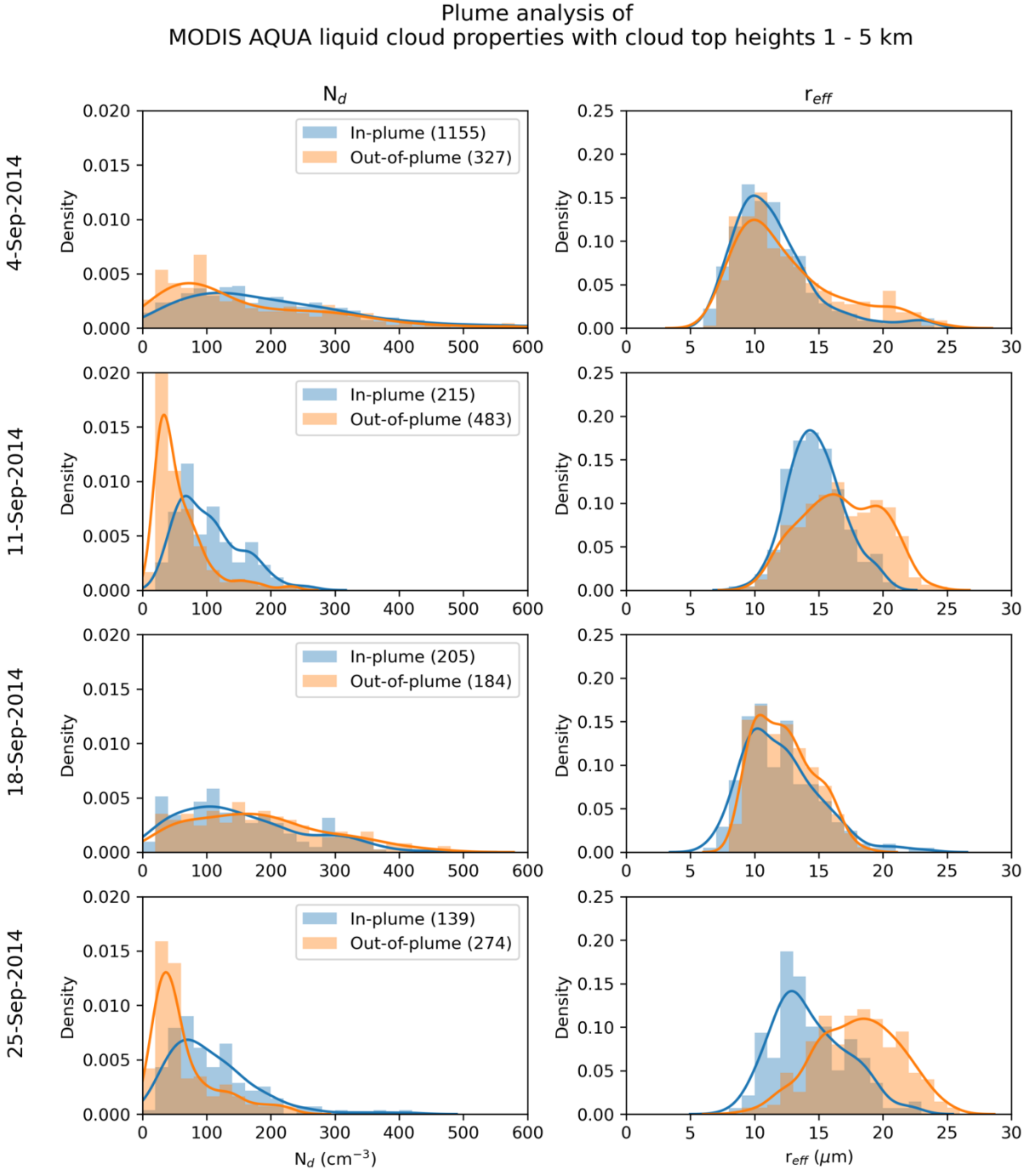

Figure 3: Histogram of MODIS AQUA liquid cloud droplet number concentration (left column) and effective radius (right column) in-plume (blue) and out-of-plume (orange) within the bounding box region for snapshot midweek days in September 2014. Only marine cloud properties with cloud top heights between 1-5 km are evaluated. The number of in-plume and out-of-plume data points are displayed.

https://doi.org/10.5194/egusphere-2024-360
Preprint. Discussion started: 8 February 2024

2.2 Aerosol perturbation to observed in-plume cloud properties

The next stage of our analysis compares cloud properties retrieved from MODIS AQUA inside the SO_2 plume mask to areas outside the plume mask yet still within the bounding region. Supplementary Figure S1 shows the plume mask bounding region overlaid on MODIS observations of marine liquid cloud N_d and r_{eff} for our snapshot days. This figure gives an indication of the spatial variation in cloud properties across the domain and the data coverage when we isolate liquid clouds with cloud top heights of 1 to 5 km.

We evaluate if there is an aerosol induced perturbation to N_d, r_{eff}, and LWP in marine liquid clouds for days in September 2014 when both OMPS and MODIS observations are available. Animations of daily cloud properties and their in-plume vs out-of-plume distribution are shown in Supplementary Animations S3-S5. As an example of the daily analysis, Figure 3 shows the distribution of N_d and r_{eff} in-plume and out-of-plume for our snapshot days. For each day we use the Mann-Whitney U test (Mann and Whitney, 1947) to evaluate if the sample of in-plume cloud properties is significantly different to the sample of the out-of-plume cloud properties. The results of this statistical significance test are summarised in Figure 4.

In over half the days we analyse (13 out of 22) observed N_d is statistically significantly higher inside the plume compared to outside. Between the 1st to 12th September there is only one day (7th September) where N_d is not higher within the plume. However, between 14th and 19th September no days display significantly higher N_d inside the plume. If we exclude 14th September due to its small sample size (supplementary Figure S5), the remaining days in this collection fall within the 3rd week of September; later in the study we aggregate our results into the weeks of September. In the 4th week of September, 4 of the 6 days analysed have significantly higher N_d within the plume. All the days that display significantly larger values of N_d in-plume have corresponding statistically significantly smaller values of r_{eff} in-plume. An aerosol induced increase in N_d and decrease in r_{eff} is consistent with the Twomey effect (Twomey, 1974) which has been widely observed (e.g. Christensen et al., 2022). Most days (6 out of 8) within the first two weeks of September that have an increase in in-plume N_d show a significant increase in LWP. No days within the first two weeks show a significant decrease in LWP. Yet the days in the 4th week of September that display an in-plume increase in N_d reveal a different picture for the LWP response. Two thirds of these days (4 out of 6) show a decrease of in-plume LWP.

To investigate the lack of perturbation to the in-plume N_d for many days of the 3rd week of September and why there is a variation in the in-plume LWP response across September, we aggregate our daily plume analysis into the weeks of September. We also use the weekly-aggregated data to compare the observed in-plume perturbation to cloud properties to that simulated by UKESM1-A. Figure 5 shows the weekly in-plume and out-of-plume distributions for N_d and r_{eff}. LWP is shown in Figure S2. The weekly aggregated results confirm our daily plume analysis; there is a statistically significant increase in N_d and decrease in r_{eff} for the 1st, 2nd and 4th weeks of September, which is absent in the 3rd week. The sample of in-plume LWP is

https://doi.org/10.5194/egusphere-2024-360
Preprint. Discussion started: 8 February 2024

statistically significantly greater in the first two weeks of September, but not in the last week. However, the mean in-plume enhancement in LWP during the first two weeks is negligible (slightly negative) which results from a decrease in frequency of low and very high values of LWP and an increase in frequency of mid to high values of LWP inside the plume. We next compare our observed weekly plume analysis results to those from UKESM1-A and use diagnostics available from the model simulations in combination with airmass back trajectory analysis to untangle the differences in the aerosol-perturbation to cloud properties over the first four weeks of the Holuhruan eruption.

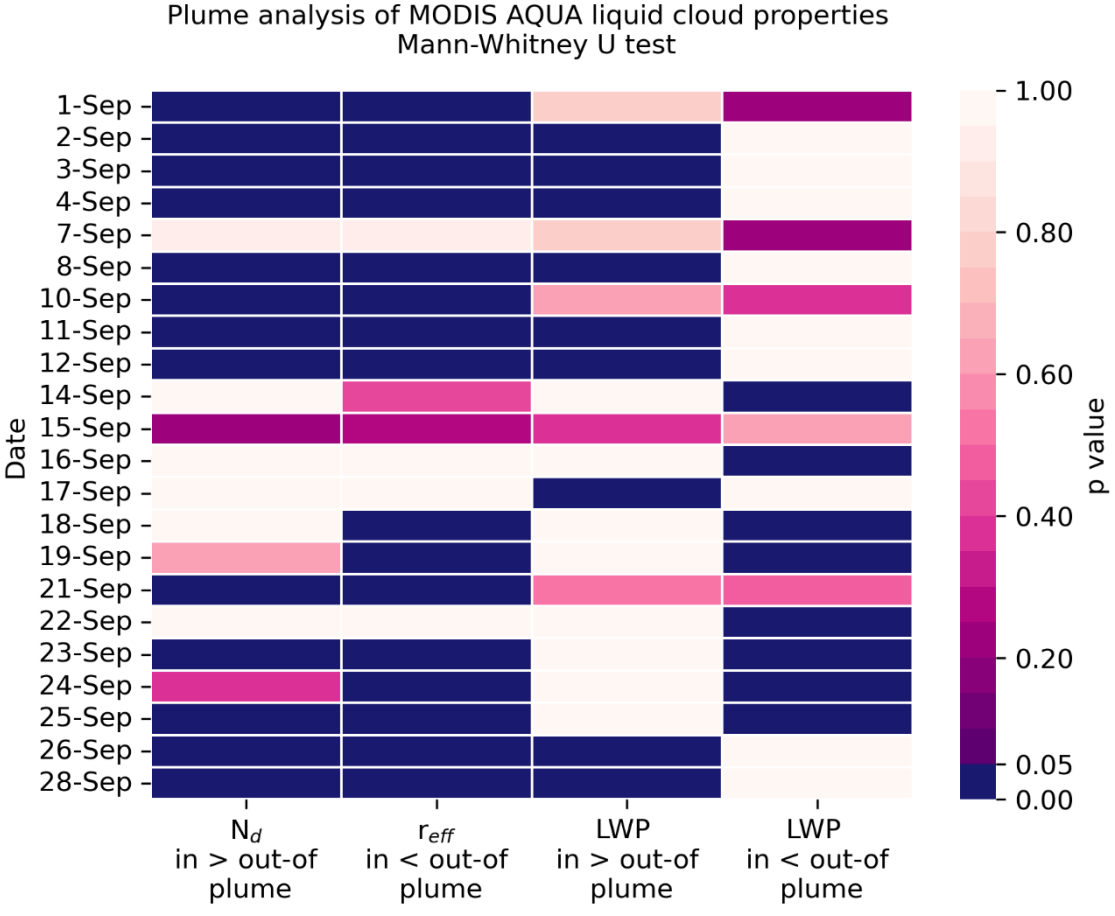

Figure 4: Statistical significance of daily changes in observed cloud properties inside vs outside of the SO_2 plume mask. Significance is evaluated using the Mann-Whitney U test. The colour bar displays the p value, with dark blue indicating a statistically significant perturbation to cloud properties inside the plume for that day.

https://doi.org/10.5194/egusphere-2024-360
Preprint. Discussion started: 8 February 2024

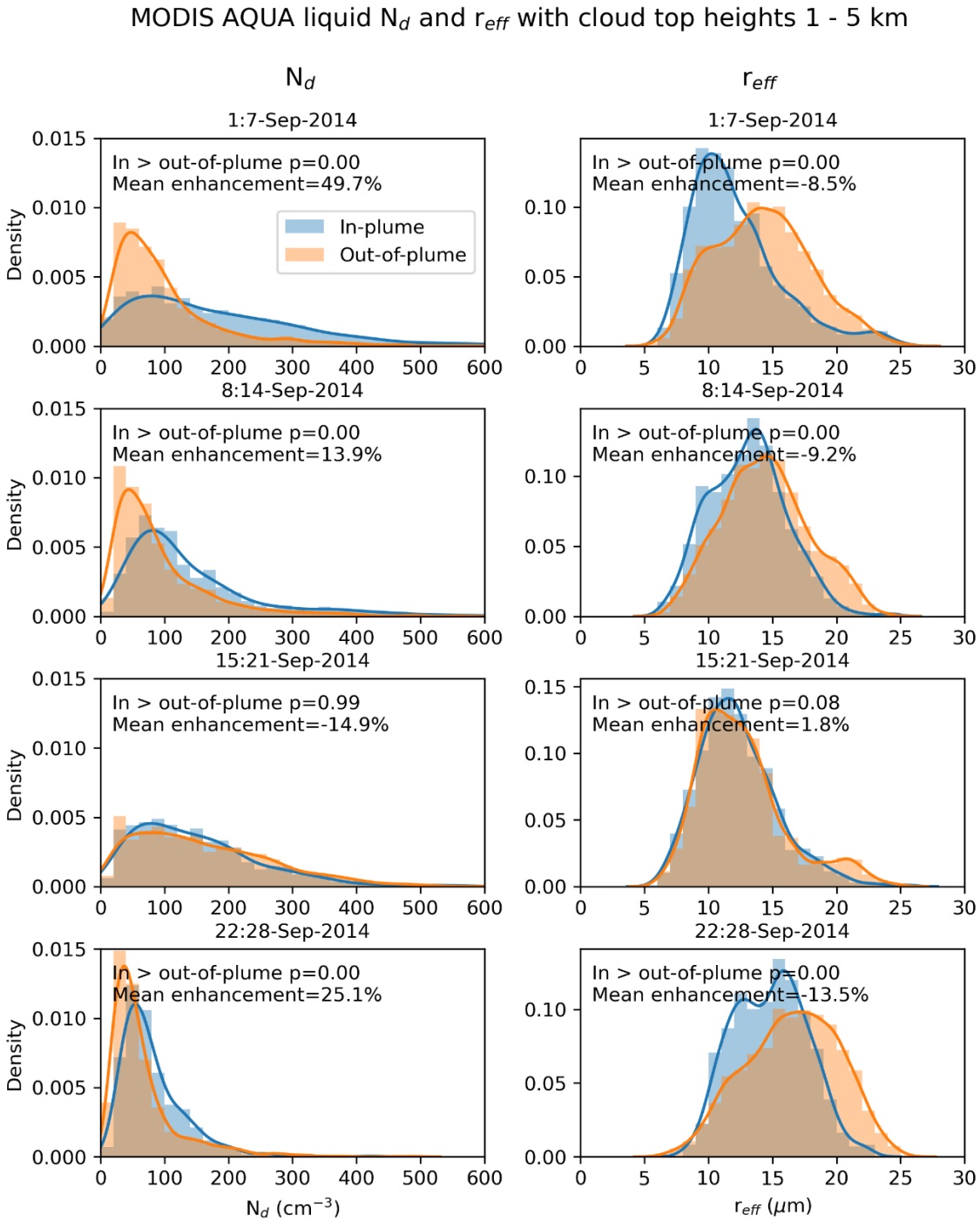

Figure 5: Histogram of MODIS AQUA liquid cloud droplet number concentration (cm^{-3}) and effective radius (μm) inside (blue) and outside (orange) the plume mask aggregated by week. Only cloud properties over sea with cloud top heights between 1-5 km are considered. The Mann-Whitney U test is used to calculate if the in-plume Nd is statistically higher than outside of the plume. The p value and mean in-plume enhancement is displayed for each week.

https://doi.org/10.5194/egusphere-2024-360
Preprint. Discussion started: 8 February 2024

2.3 Comparison of observed vs modelled perturbation to in-plume cloud properties

Table 1 shows the regional mean values of liquid cloud properties inside and outside of the plume mask, and the corresponding mean in-plume perturbation to cloud properties. The UKESM1-Hol simulation shows significantly greater N_d and significantly smaller r_{eff} inside the plume in the first two weeks of September, with no statistically significant perturbation in the control simulation. The lack of perturbation to N_d and r_{eff} in UKESM1-Ctrl indicates the perturbation to cloud properties inside the plume is not explained by meteorological variability and is therefore aerosol-induced. In the 3rd week, UKESM1-Hol features no significant perturbations to N_d and r_{eff} which is in-line with our results from MODIS, and indicates the reason for the lack of observed perturbation to N_d is represented in UKESM1-A. In the 4th week there is not a significant increase in N_d or decrease in r_{eff} in UKESM1-Hol or UKESM1-Ctrl, despite the presence of these perturbations in the MODIS observations. The statistical significance of daily changes in modelled cloud properties is summarised in Figure S4.

There is not a significant increase or decrease in in-plume LWP in UKESM1-Hol during the first two weeks of September. This contrasts with MODIS where the distribution of in-plume LWP values is significantly greater than out-of-plume. However, in both simulations and observations, the in-plume mean change in LWP is small during the first two weeks. In the 3rd week, there is an observed decrease in LWP inside the plume. The in-plume decrease in LWP is represented in the eruption and control simulations, indicating that the decrease in LWP in the 3rd week could be due to the sampling of different cloud conditions inside the plume rather than an aerosol effect. During the 4th week there is a mean in-plume reduction in LWP in MODIS, although the sample of LWP values inside the plume is not statistically significantly lower than outside the plume. Any reduction in LWP during the 4th week is not reproduced in the UKESM1-Hol simulations.

These results indicate that UKESM1-A captures the observed change in N_d and r_{eff} in the first two weeks of September 2014 but there is not a significant change in simulated in-plume LWP during these two weeks. The model control simulations help elucidate that changes in cloud properties inside the plume during the 3rd week are likely not due to ACI. Next, we use the UKESM1-Hol simulation and trajectory modelling to investigate the aerosol-cloud interaction mechanisms at play during the different weeks in September 2014.

https://doi.org/10.5194/egusphere-2024-360
Preprint. Discussion started: 8 February 2024

		Inside (outside) plume values				In-plume perturbation (%)			
Week		1	2	3	4	1	2	3	4
N_d (cm^{-3})	MODIS	144 (96)	121 (107)	142 (167)	78 (63)	50	14	-15	25
	UKESM-Hol	252 (159)	260 (216)	181 (198)	226 (219)	59	21	-9	3
	UKESM-Ctrl	102 (115)	96 (106)	101 (133)	113 (108)	-12	-10	-25	4
r_{eff} (μm)	MODIS	13.4 (14.6)	12.8 (14.1)	12.7 (12.5)	14.5 (16.7)	-9	-9	2	-14
	UKESM-Hol	10.0 (11.5)	9.4 (9.9)	10.7 (10.0)	10.7 (11.6)	-13	-5	7	-8
	UKESM--Ctrl	12.4 (12.3)	11.8 (11.8)	12.1 (11.5)	12.6 (12.4)	1	-1	5	1
LWP ($g\ m^{-2}$)	MODIS	171 (172)	172 (179)	174 (223)	153 (199)	-1	-4	-22	-23
	UKESM-Hol	136 (138)	103 (99)	96 (125)	171 (140)	-1	5	-23	22
	UKESM-Ctrl	124 (117)	76 (82)	78 (119)	103 (121)	6	-7	-34	-15
cloud fraction (%)	MODIS	96.7 (93.7)	88.3 (91.6)	93.4 (96.1)	91.8 (89.8)	3	-4	-3	2

Table 1: Weekly means of the area-weighted regional mean of MODIS and UKESM1-A liquid cloud properties inside and outside of the plume mask. The last four columns display the mean in-plume perturbation (%) of each cloud property. The in-plume perturbation is calculated daily as (area mean inside plume-area mean outside of plume)/area mean outside of plume. The daily in-plume enhancement is then averaged to obtain the in-plume perturbation for each week. The blue and green shading indicates where weekly aggregated in-plume values are respectively statistically greater or less than outside of the plume.

https://doi.org/10.5194/egusphere-2024-360
Preprint. Discussion started: 8 February 2024

2.4 Disentangling aerosol-cloud interaction mechanisms during September 2014

In the previous section we showed that the lack of in-plume perturbation to N_d and r_{eff} in the 3rd week of September featured in both the MODIS observations and the UKESM1-A Holuhraun simulation. In the 3rd week, the MODIS out-of-plume N_d distribution shown in Figure 5 more closely resembles the polluted in-plume distributions of N_d than the clean out-of-plume backgrounds. We use back-trajectory modelling to explore the air mass origins during the different weeks of our analysis. Figure 6 shows that during weeks 1, 2 and 4 back trajectories initialised at the eruption site mostly pass through pristine air to the west of Iceland enroute to the Holuhraun eruption site. However, in week 3, a larger proportion of the back-trajectories pass over Western Europe. The air masses passing over Europe will experience greater aerosol pollution from anthropogenic sources, which is a plausible reason for higher background N_d during week 3. This polluted background is also well simulated by UKESM1-A (Figure S5). In addition, CCN activation and cloud droplet formation can occur under updraft-limited, aerosol-limited or aerosol- and updraft-sensitive regimes (Reutter et al., 2009). The updraft-limited activation regime is more likely to occur under polluted air masses, such as week 3 in our analysis (Jones et al., 1994; Reutter et al., 2009; Carslaw et al., 2013; Spracklen and Rap, 2013). As a result, polluted air masses arriving in the region of the Holuhraun aerosol plume during the 3rd week would be less susceptible to further aerosol-induced increases in N_d.

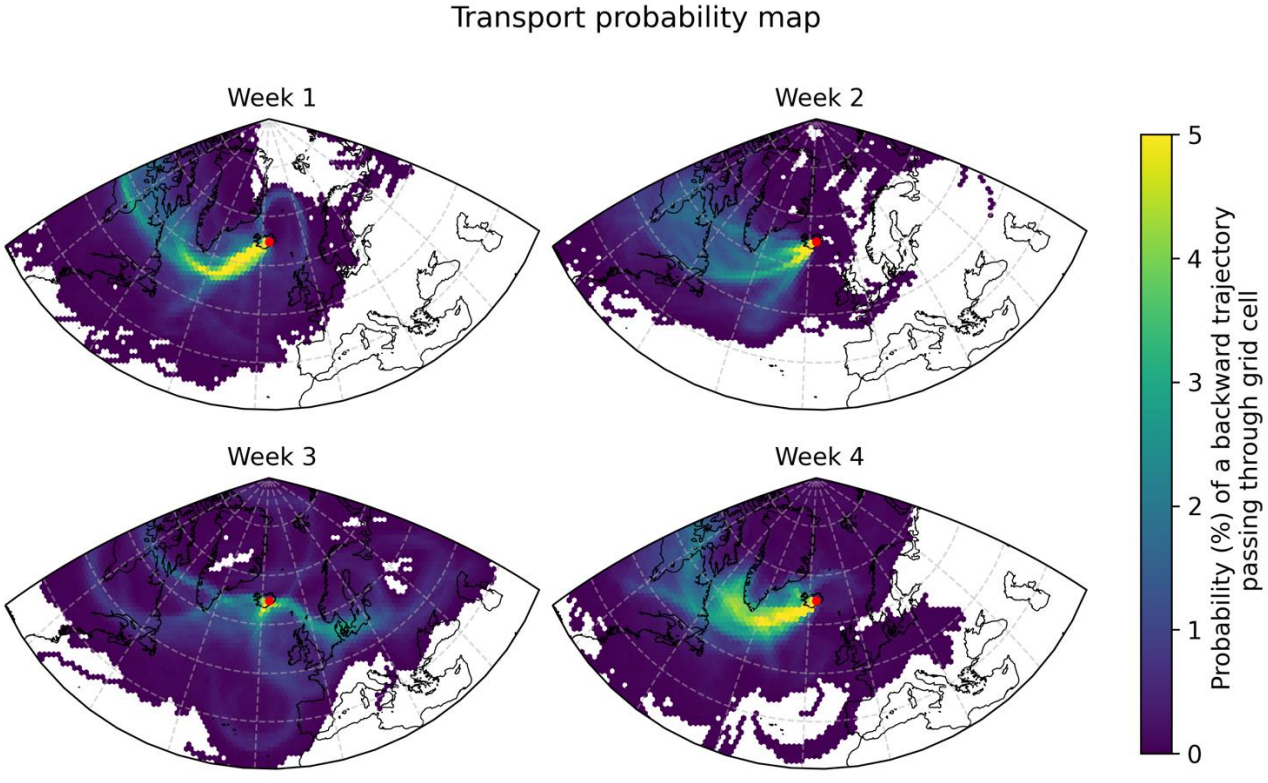

Figure 6: An ensemble of back trajectories was initialised each hour at 2000 m above the Holuhraun eruption site (64.85°N, 16.83°W), as explained in Section 2.4. The probability (%) of a backward trajectory passing through a specific grid cell ($A_{i,j}$) is shown here. The start dates of the trajectories are grouped by the weeks of our analysis.

https://doi.org/10.5194/egusphere-2024-360
Preprint. Discussion started: 8 February 2024

We also explore if the meteorological conditions during the weeks of our analysis affect ACI. During week 3, the MODIS in-plume LWP and cloud fraction is lower than outside the plume. In the absence of a clear aerosol-cloud interaction inside the Holuhraun plume, a difference in LWP and cloud fraction may indicate the area inside the plume has different meteorological conditions and cloud properties to outside of the plume. Figure 7 shows visible satellite imagery in the 3rd week overlayed by the plume mask and bounding box region. On 16th – 19th September there is a region of clear sky that persists in the north of the bounding box. Since there is agreement between the observations and simulations in the 3rd week, we use the UKESM1-Hol simulation to investigate differences in meteorological conditions during the 3rd week that may contribute towards the negligible in-plume aerosol perturbation to cloud properties.

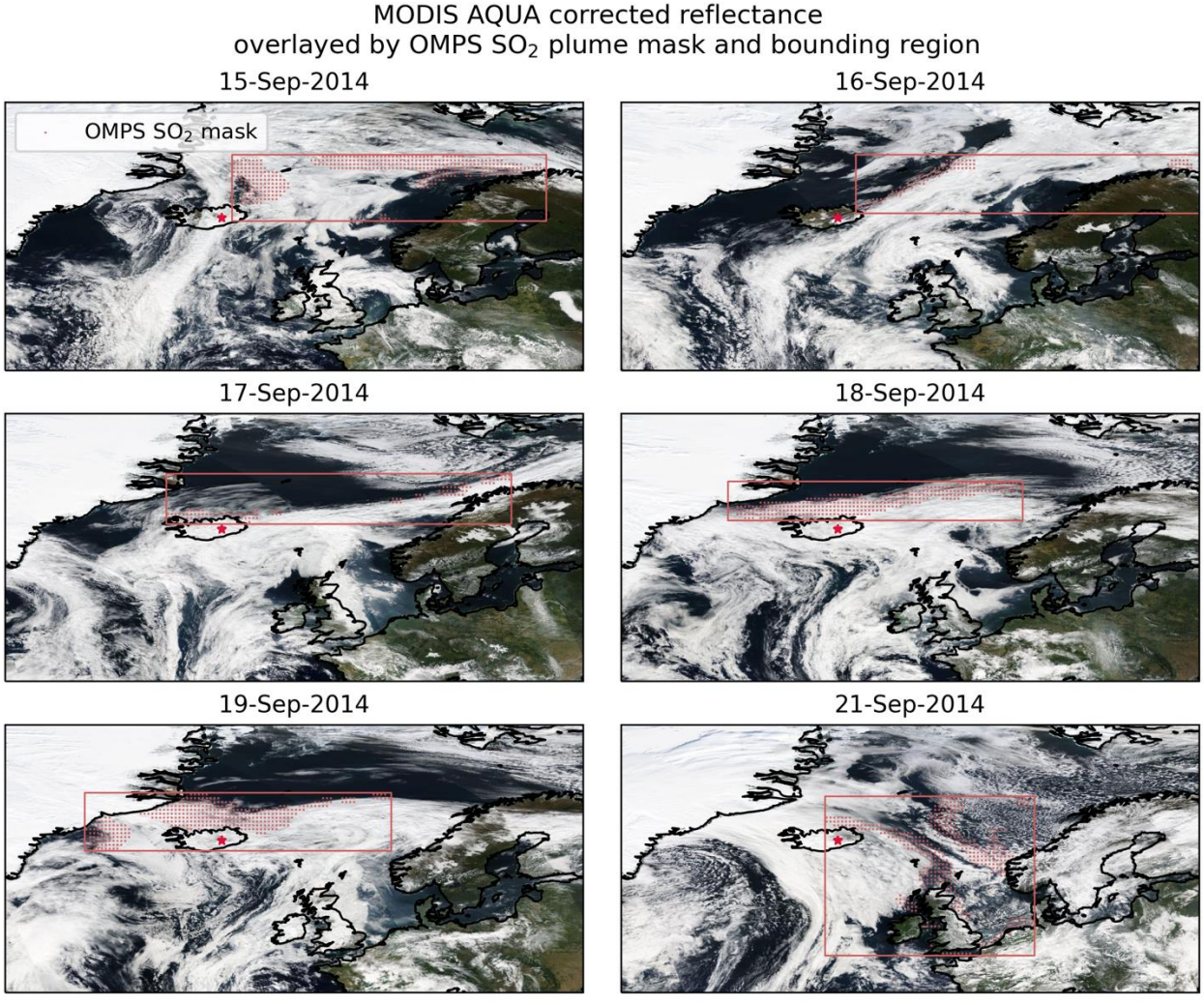

Figure 7: Visible image from MODIS AQUA for 15th – 21st September 2014. The OMPS SO_2 plume mask and bounding region is overlaid on the visible imagery. 20th September is excluded due to no OMPS SO_2 retrieval on that day. Visible imagery is obtained from the corrected reflectance (true colour) MODIS AQUA data available on NASA Worldview (https://worldview.earthdata.nasa.gov/, last access 1st June 2023).

https://doi.org/10.5194/egusphere-2024-360
Preprint. Discussion started: 8 February 2024

Figure 8 shows meteorological variables inside the bounding box in the UKESM1-Hol simulation. The 3rd week is noticeably drier in terms of precipitation and relative humidity at 950 hPa which is representative of the clear-sky region in the north of the bounding box during the 16th – 19th September. There is a slightly lower median and smaller interquartile range of lower tropospheric stability (LTS) during the 3rd week but there are many outliers that represent grid cells with higher LTS values. The number of outliers with high LTS values implies a contrast in the conditions in the bounding box during 3rd week. A higher LTS value indicates a strong, low-lying inversion that traps moisture more efficiently in the boundary layer and favours greater cloud cover (Wood and Bretherton, 2006).

Variables affecting the production of sulphate aerosol and the number of aerosols activated to cloud droplets are also shown in Figure 8. The first box plot shows the ratio of vertical mean gas-phase to aqueous-phase production rate of sulphate aerosol (SO_4^{2-}) inside the plume. The median and quartiles of the ratio have higher values in week 3. A higher ratio indicates either more gas-phase production or less aqueous-phase production of sulphate which is consistent with the plume location partly covering a region with less cloud during week 3. In the gas-phase, sulphate aerosol is formed through the reaction of SO_2 with OH to form H_2SO_4 vapour. Nucleation and condensation then occur to produce aerosols with larger size and number. In UKESM1, these gas-phase aerosol processes produce sulphate aerosol in all size modes whereas in clouds, SO_2 dissolves and undergoes oxidation with H_2O_2 and O_3 to form sulphate (Turnock et al., 2019). The sulphate aerosol produced through in-cloud oxidation is split into the soluble accumulation and coarse modes (Mulcahy et al., 2020). Less aqueous-phase production of sulphate aerosol is therefore in line with the lower values of in-plume soluble accumulation mode aerosol (i.e. an effective size for droplet nucleation) during week 3. The magnitude of SO_2 emissions in the Holuhraun simulations follow that described in Malavelle et al., 2017 (as shown in their Supporting Information). Emissions during the first two weeks of the eruption were larger than during weeks 3 and 4 which also contributes to lower amount of soluble accumulation mode aerosol during these weeks in the Holuhraun simulations. However, emissions were still large at 57.5 kT SO_2/day during the latter weeks and we would expect an aerosol perturbation to N_d in an environment susceptible to aerosol perturbation.

Accumulation mode aerosol dominate the contribution to CCN concentrations over polluted land regions (e.g. Chang et al., 2017). In UKESM1, aerosols are activated into cloud droplets using the activation scheme of Abdul-Razzak and Ghan, 2000. Once per timestep the activation scheme calculates N_d at cloud base and imposes it on all grid cells above the cloud base within the same liquid cloud. The activation scheme also depends on the subgrid vertical velocity variance (West et al., 2014). The box plots shows that although soluble accumulation mode aerosol is lower during the last two weeks of September than the first two weeks, the difference in the number of activated particles at the lowest cloud base in the bounding region is less evident. In an updraft-limited activation regime that is more likely to occur under polluted air masses (such as week 3), cloud droplet formation is proportional to updraft velocity and essentially independent of aerosol number concentration (Reutter et al., 2009). The last two weeks of September exhibit larger variance in subgrid vertical velocity at the lowest cloud base. Hence, an updraft-limited regime would explain why week 3 has a similar number of activated particles at the lowest cloud base

https://doi.org/10.5194/egusphere-2024-360
Preprint. Discussion started: 8 February 2024

compared to other weeks despite lower accumulation mode aerosol inside the bounding box. Haghighatnasab et al. (2022) showed how increasing the updraft velocity can increase the background CCN concentration in the Holuhraun domain in a cloud-resolving model. Yet, further study would be needed to definitively identify the activation regime during each week of our study to support these results.

The LWP response to an increase in N_d likely depends on the meteorological conditions present, as noted in the introduction. Our results show a shift in the distribution of MODIS LWP inside the plume during weeks 1 and 2 that results from more values in the range ~ 100-300 g m^{-2} and less values ~ < 100 g m^{-2} inside the plume. An increase in LWP is traditionally associated with reduced collision coalescence in clouds with smaller droplets that can delay the onset of precipitation and result in the accumulation of in-cloud water content (Pincus and Baker, 1994). LWP has been found to increase in low precipitating marine liquid clouds below moist air; whereas in thicker, non-precipitating clouds below dry air there may be a decrease in LWP (Toll et al., 2019). The simulations show that humid conditions are present during week 1 and 2 and some clouds are likely to be precipitating (indicated by reff > 14 µm as shown in Figure 3 and Animation S4) which would be in support of conditions favourable for an increase LWP. The in-plume LWP in the Holuhraun simulation were not significantly greater or less than the values out-of-plume during weeks 1 and 2, which contrasts with climate models' tendency to produce unrealistic high LWP increase when N_d increases (e.g. Malavelle et al., 2017). We do not discuss the LWP response in weeks 3 and 4 further here due to the missing causal processes of ACI in week 3 and the insignificant observed and modelled LWP response in week 4.

https://doi.org/10.5194/egusphere-2024-360
Preprint. Discussion started: 8 February 2024

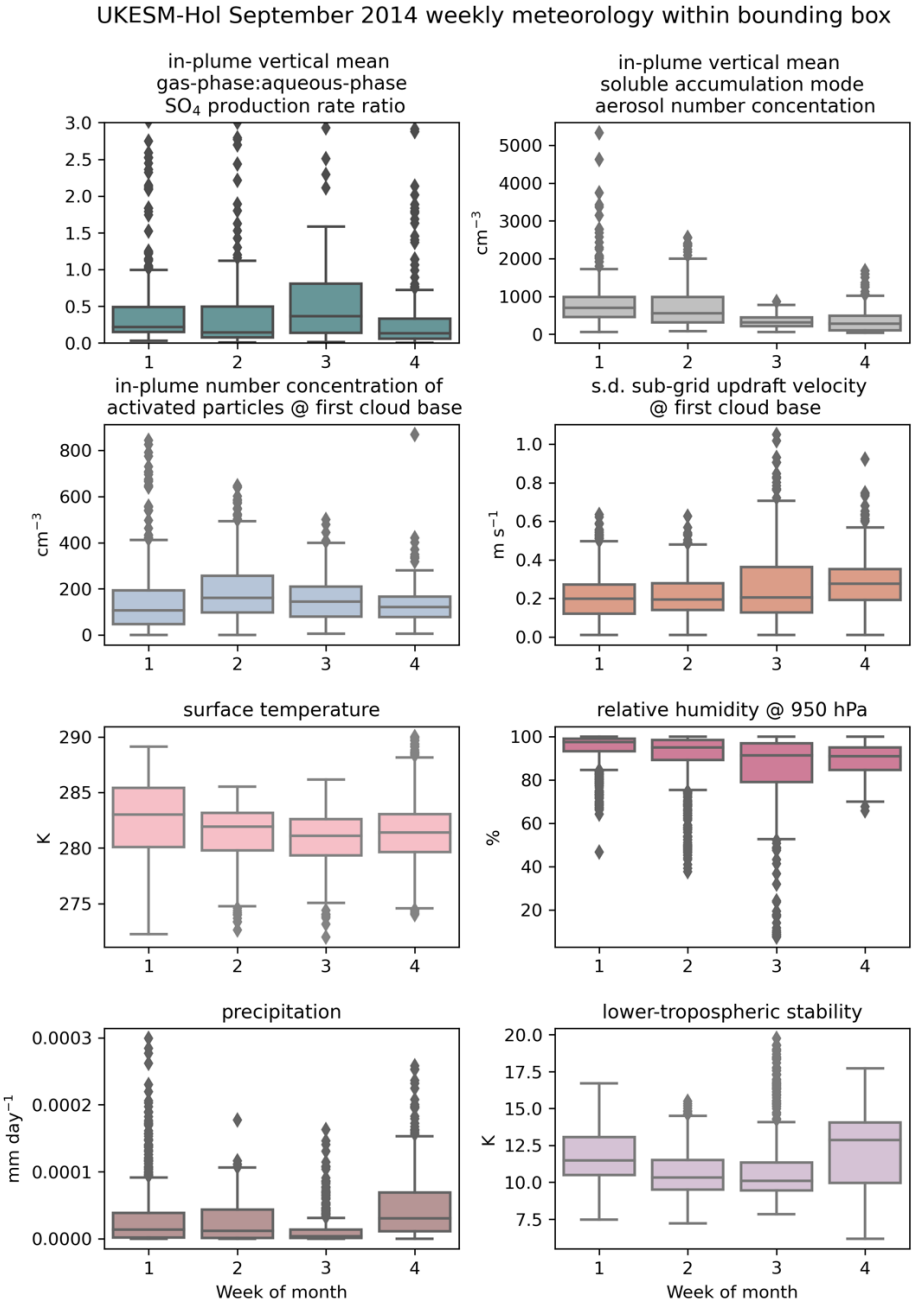

420 **Figure 8: Box plots of meteorological variables within the plume mask bounding box from the UKESM-Hol simulation. The variables shown are ratio of vertical mean gas-phase to aqueous phase production rate of SO_4, vertical mean soluble accumulation mode aerosol number concentration, number concentration of activated particles at first cloud base, standard deviation of sub-grid updraft velocity at first cloud base, surface temperature, precipitation, relative humidity at 950 hPa and lower-tropospheric stability. The daily mean data within the bounding box are aggregated into the four weeks. The first 3 box plots show the in-plume values.**
425 **The y axis of the SO_4 production rate ratio was adjusted to show the box as there was outliers with high values. The box plots show the interquartile range and the median, with the whiskers denoting 1.5 times the interquartile range, and outliers that are defined as outside this range shown as diamond points.**

https://doi.org/10.5194/egusphere-2024-360
Preprint. Discussion started: 8 February 2024

4 Discussion and conclusions

Opportunistic experiments with a known aerosol source, such as degassing volcanic eruptions, offer a way to investigate aerosol-cloud interactions (e.g. Christensen et al., 2022). Our study has built on previous analyses of ACI following the 2014-15 Holuhraun eruption (McCoy and Hartmann, 2015; Malavelle et al., 2017; Chen et al., 2022; Haghighatnasab et al., 2022). We utilise an in-plume versus out-of-plume analysis approach to isolate aerosol perturbations to cloud properties in satellite observations and UKESM1-A simulations, and trajectory modelling to understand the impact of airmass history on ACI. Particularly we build on the study of Haghighatnasab et al. 2022 who also used a plume analysis approach, but we use a more detailed plume tracking method and extend the plume analysis approach to the rest of September. The extension of the analysis time frame allows us to group our analysis into weeks that experience differing airmass history and meteorological conditions and elucidate their role on ACI.

We have shown during the first two weeks of September that there is an increase in N_d and decrease in r_{eff}, observed, and simulated by UKESM1-Hol when the eruption aerosol plume likely interacts with liquid clouds. As expected, the increased N_d and decreased r_{eff} inside the plume are not reproduced in UKESM1-Ctrl, indicating the perturbation is due to ACI and not differences in meteorology. Our results, which reveal an increase in N_d and decrease in r_{eff} due to Holuhraun eruption aerosol plume are in line with previous ACI studies of the eruption (McCoy and Hartmann, 2015; Malavelle et al., 2017; Haghighatnasab et al., 2022; Chen et al., 2022). However, during the 3rd week in September an increase in N_d is neither observed nor modelled. In the 4th week of September, we observe an increase in N_d and decrease in r_{eff}, but an insignificant change in the simulations. To understand what caused the different responses of clouds to increased aerosol across the weeks of our analysis, we used trajectory modelling to track the air mass history in the region, alongside assessing the meteorology and activation of aerosols into cloud droplets using the UKESM1-A simulations.

The 10-day back trajectories reveal that air masses arriving at the Holuhraun eruption site during the 3rd week will likely be more polluted than the other weeks due to passing over Western Europe rather than originating in pristine regions. Polluted air masses are also more likely to experience updraft-limited rather than aerosol-limited CCN activation (Reutter et al., 2009). Hence, the conditions in the 3rd week may be less susceptible to further aerosol-induced increases in N_d than the other weeks of our analysis due to the polluted background (e.g. Jones et al., 1994; Carslaw et al., 2013). The meteorological fields in the UKESM1-Hol simulation show the 3rd week is drier in terms of relative humidity and precipitation, with the satellite imagery indicating a region of persistent clear-sky in the north of the bounding box region the likely cause. The meteorological conditions during the 3rd week therefore support the higher ratio of gas-phase to in-cloud production of sulphate aerosol which produced less soluble accumulation mode aerosol in the 3rd week, the dominate aerosol mode in the contribution to CCN concentrations over polluted land regions. Overall, we therefore conclude that a combination of the airmass history and background meteorological factors strongly influence aerosol-cloud interactions in the third week. The ability of background

https://doi.org/10.5194/egusphere-2024-360
Preprint. Discussion started: 8 February 2024

N_d and meteorology in the modulation of ACI, illustrates the importance of improving knowledge of background conditions for accurately calculating ACI. For example, the pre-industrial aerosol loading is a dominant source of uncertainty in present-day aerosol ERF (Carslaw et al., 2013), and present-day analogues to pristine environments can contribute towards constraining aerosol forcing uncertainty (McCoy et al., 2020b; Regayre et al., 2020).

We assessed the LWP response in the first two weeks where we isolated an observed and modelled shift to smaller and more numerous liquid cloud droplets inside the aerosol plume. We find an observed decrease in the likelihood of small LWP values (< ~100 g m^{-2}) and increase in likelihood of LWP values in the range of ~100-300 g m^{-2} inside the plume, resulting in a negligible mean in-plume perturbation to LWP. While Malavelle et al. 2017 and Chen et al. 2022 did not isolate an observed perturbation to LWP in monthly means, Haghighatnasab et al., 2022 showed an in-plume decrease in the probability of values with low LWP and an increase of values with high LWP in satellite observation and cloud-resolving simulations for the 1st week, which is consistent with our results. Cloud-resolving simulations of the Holuhraun eruption suggest there is a decrease in light rain and increase in heavy rain (Haghighatnasab et al., 2022). A decrease in light rain may be due to reduced collision coalescence of smaller droplets that can delay precipitation, and lead to droplets growing larger in size before precipitating, increasing heavy rain and shifting the distribution of in-plume LWP values (Fan et al., 2016; Haghighatnasab et al., 2022). This mechanism of an increase in LWP due to precipitation suppression supports our observed increase in LWP values inside the plume during the first two weeks of September. However, in UKESM1-Hol, the distribution of LWP values in-plume is not significantly different to out-of-plume. Malavelle et al. 2017 showed that HadGEM3-UKCA (a previous generation of the aerosol-climate model used in UKESM1) produced a minimal LWP response following the Holuhraun eruption, but that models generally overestimate the increase in LWP due to increased aerosol (Malavelle et al., 2017; Toll et al., 2017).

To conclude, the causal chain of events highlighted over two decades ago (e.g. Haywood and Boucher, 2000) of increases in cloud droplet number concentration decreasing cloud effective radius (Twomey, 1974), which delays auto-conversion and precipitation processes leading to greater cloud liquid water (Albrecht, 1989) appears to apply in this study. Because our study targets the impacts of aerosols on clouds from an observational basis using an in-plume/out-of-plume mask, it cannot explicitly account for changes in cloud fraction. Significant changes in cloud fraction have been demonstrated for the Holuhraun eruption using a machine-learning approach (Chen et al., 2022). We recommend that ensembles of climate model simulations (e.g. Jordan et al. 2023), higher resolution nested simulations and a more comprehensive use of a Lagrangian framework (e.g. Coopman et al., 2018,) of this opportunistic experiment would provide a more detailed assessment on the causality of meteorological conditions affecting the aerosol perturbation to cloud properties.

https://doi.org/10.5194/egusphere-2024-360
Preprint. Discussion started: 8 February 2024

Code and data availability

The MODIS cloud and products from Aqua (MYD08_L2) used in this study are available from the Atmosphere Archive and Distribution System Distributed Active Archive Center of National Aeronautics and Space Administration (LAADS-DAAC, NASA), https://ladsweb.modaps.eosdis.nasa.gov. The OMPS SO_2 (OMPS_NPP_NMSO2_PLC_L2 v2) data used in this study is available to download from GES-DISC, NASA, https://disc.gsfc.nasa.gov/datasets/OMPS_NPP_NMSO2_PCA_L2_2/summary. Simplified data and code required to reproduce the main figures in this article will be provided on Zonodo (link placeholder).

Author contributions

AP and JH designed the study. Gridded MODIS data was created from Level 2 products by YC. GJ ran the model simulations. ED and DP provided guidance in the use of HYSPLIT trajectories. Data analysis and figure preparation was completed by AP. All co-authors provided discussion on the interpretation of results. AP wrote the manuscript with advice from all co-authors.

Acknowledgments

JH, DP, YC, AP, and ED would like to acknowledge funding from the NERC ADVANCE grant (NE/S015671/1). GJ and JH were funded under the European Union's Horizon 2020 research and innovation programme under the CONSTRAIN grant agreement 820829. GJ, JH and FM are supported by the Met Office Hadley Centre Climate Programme funded by BEIS. DP would like to express his gratitude to Zak Kipling for providing support in obtaining HYSPLIT input files from ERA-Interim reanalysis data. We would like to thank Paul Kim who helped develop the running and plotting framework for HYSPLIT trajectories and Andy Jones for helping with the experimental set up of UKESM1. We acknowledge the use of imagery from the NASA Worldview application (https://worldview.earthdata.nasa.gov), part of the NASA Earth Observing System Data and Information System (EOSDIS).

Competing interests

The authors declare that they have no conflicts of interest.

https://doi.org/10.5194/egusphere-2024-360
Preprint. Discussion started: 8 February 2024

References

Abdul-Razzak, H. and Ghan, S. J.: A parameterization of aerosol activation: 2. Multiple aerosol types, Journal of Geophysical Research: Atmospheres, 105, 6837–6844, https://doi.org/10.1029/1999JD901161, 2000.

Ackerman, A. S., Kirkpatrick, M. P., Stevens, D. E., and Toon, O. B.: The impact of humidity above stratiform clouds on indirect aerosol climate forcing, Nature, 432, 1014–1017, https://doi.org/10.1038/nature03174, 2004.

Albrecht, B. A.: Aerosols, Cloud Microphysics, and Fractional Cloudiness, Science, 245, 1227–1230, https://doi.org/10.1126/science.245.4923.1227, 1989.

Andreae, M. O., Jones, C. D., and Cox, P. M.: Strong present-day aerosol cooling implies a hot future, Nature, 435, 1187–1190, https://doi.org/10.1038/nature03671, 2005.

Archibald, A. T., O'Connor, F. M., Abraham, N. L., Archer-Nicholls, S., Chipperfield, M. P., Dalvi, M., Folberth, G. A., Dennison, F., Dhomse, S. S., Griffiths, P. T., Hardacre, C., Hewitt, A. J., Hill, R. S., Johnson, C. E., Keeble, J., Köhler, M. O., Morgenstern, O., Mulcahy, J. P., Ordóñez, C., Pope, R. J., Rumbold, S. T., Russo, M. R., Savage, N. H., Sellar, A., Stringer, M., Turnock, S. T., Wild, O., and Zeng, G.: Description and evaluation of the UKCA stratosphere–troposphere chemistry scheme (StratTrop vn 1.0) implemented in UKESM1, Geoscientific Model Development, 13, 1223–1266, https://doi.org/10.5194/gmd-13-1223-2020, 2020.

Bellouin, N., Quaas, J., Gryspeerdt, E., Kinne, S., Stier, P., Watson-Parris, D., Boucher, O., Carslaw, K. S., Christensen, M., Daniau, A.-L., Dufresne, J.-L., Feingold, G., Fiedler, S., Forster, P., Gettelman, A., Haywood, J. M., Lohmann, U., Malavelle, F., Mauritsen, T., McCoy, D. T., Myhre, G., Mülmenstädt, J., Neubauer, D., Possner, A., Rugenstein, M., Sato, Y., Schulz, M., Schwartz, S. E., Sourdeval, O., Storelvmo, T., Toll, V., Winker, D., and Stevens, B.: Bounding Global Aerosol Radiative Forcing of Climate Change, Reviews of Geophysics, 58, e2019RG000660, https://doi.org/10.1029/2019RG000660, 2020.

Bodas-Salcedo, A., Webb, M. J., Bony, S., Chepfer, H., Dufresne, J.-L., Klein, S. A., Zhang, Y., Marchand, R., Haynes, J. M., Pincus, R., and John, V. O.: COSP: Satellite simulation software for model assessment, Bulletin of the American Meteorological Society, 92, 1023–1043, https://doi.org/10.1175/2011BAMS2856.1, 2011.

Boichu, M., Chiapello, I., Brogniez, C., Péré, J.-C., Thieuleux, F., Torres, B., Blarel, L., Mortier, A., Podvin, T., Goloub, P., Söhne, N., Clarisse, L., Bauduin, S., Hendrick, F., Theys, N., Van Roozendael, M., and Tanré, D.: Current challenges in modelling far-range air pollution induced by the 2014–2015 Bárðarbunga fissure eruption (Iceland), Atmospheric Chemistry and Physics, 16, 10831–10845, https://doi.org/10.5194/acp-16-10831-2016, 2016.

Bréon, F.-M., Tanré, D., and Generoso, S.: Aerosol Effect on Cloud Droplet Size Monitored from Satellite, Science, 295, 834–838, https://doi.org/10.1126/science.1066434, 2002.

Bretherton, C. S., Blossey, P. N., and Uchida, J.: Cloud droplet sedimentation, entrainment efficiency, and subtropical stratocumulus albedo, Geophysical Research Letters, 34, https://doi.org/10.1029/2006GL027648, 2007.

Carboni, E., Mather, T. A., Schmidt, A., Grainger, R. G., Pfeffer, M. A., Ialongo, I., and Theys, N.: Satellite-derived sulfur dioxide (SO_2) emissions from the 2014–2015 Holuhraun eruption (Iceland), Atmospheric Chemistry and Physics, 19, 4851–4862, https://doi.org/10.5194/acp-19-4851-2019, 2019.

Carslaw, K. S., Lee, L. A., Reddington, C. L., Pringle, K. J., Rap, A., Forster, P. M., Mann, G. W., Spracklen, D. V., Woodhouse, M. T., Regayre, L. A., and Pierce, J. R.: Large contribution of natural aerosols to uncertainty in indirect forcing, Nature, 503, 67–71, https://doi.org/10.1038/nature12674, 2013.

https://doi.org/10.5194/egusphere-2024-360
Preprint. Discussion started: 8 February 2024

Chang, D. Y., Lelieveld, J., Tost, H., Steil, B., Pozzer, A., and Yoon, J.: Aerosol physicochemical effects on CCN activation simulated with the chemistry-climate model EMAC, Atmospheric Environment, 162, 127–140, https://doi.org/10.1016/j.atmosenv.2017.03.036, 2017.

Chen, Y., Haywood, J., Wang, Y., Malavelle, F., Jordan, G., Partridge, D., Fieldsend, J., De Leeuw, J., Schmidt, A., Cho, N., Oreopoulos, L., Platnick, S., Grosvenor, D., Field, P., and Lohmann, U.: Machine learning reveals climate forcing from aerosols is dominated by increased cloud cover, Nat. Geosci., 15, 609–614, https://doi.org/10.1038/s41561-022-00991-6, 2022.

Christensen, M. W., Gettelman, A., Cermak, J., Dagan, G., Diamond, M., Douglas, A., Feingold, G., Glassmeier, F., Goren, T., Grosvenor, D. P., Gryspeerdt, E., Kahn, R., Li, Z., Ma, P.-L., Malavelle, F., McCoy, I. L., McCoy, D. T., McFarquhar, G., Mülmenstädt, J., Pal, S., Possner, A., Povey, A., Quaas, J., Rosenfeld, D., Schmidt, A., Schrödner, R., Sorooshian, A., Stier, P., Toll, V., Watson-Parris, D., Wood, R., Yang, M., and Yuan, T.: Opportunistic experiments to constrain aerosol effective radiative forcing, Atmospheric Chemistry and Physics, 22, 641–674, https://doi.org/10.5194/acp-22-641-2022, 2022.

Coopman, Q., Garrett, T. J., Finch, D. P., and Riedi, J.: High Sensitivity of Arctic Liquid Clouds to Long-Range Anthropogenic Aerosol Transport, Geophysical Research Letters, 45, 372–381, https://doi.org/10.1002/2017GL075795, 2018.

Dee, D. P., Uppala, S. M., Simmons, A. J., Berrisford, P., Poli, P., Kobayashi, S., Andrae, U., Balmaseda, M. A., Balsamo, G., Bauer, P., Bechtold, P., Beljaars, A. C. M., van de Berg, L., Bidlot, J., Bormann, N., Delsol, C., Dragani, R., Fuentes, M., Geer, A. J., Haimberger, L., Healy, S. B., Hersbach, H., Hólm, E. V., Isaksen, L., Kållberg, P., Köhler, M., Matricardi, M., McNally, A. P., Monge-Sanz, B. M., Morcrette, J.-J., Park, B.-K., Peubey, C., de Rosnay, P., Tavolato, C., Thépaut, J.-N., and Vitart, F.: The ERA-Interim reanalysis: configuration and performance of the data assimilation system, Quarterly Journal of the Royal Meteorological Society, 137, 553–597, https://doi.org/10.1002/qj.828, 2011.

Douville, H., K. Raghavan, J. Renwick, R.P. Allan, P.A. Arias, M. Barlow, R. Cerezo-Mota, A. Cherchi, T.Y. Gan, J. Gergis, D. Jiang, A. Khan, W. Pokam Mba, D. Rosenfeld, J. Tierney, O. Zolina: Water Cycle Changes. In Climate Change 2021: The Physical Science Basis. Contribution of Working Group I to the Sixth Assessment Report of the Intergovernmental Panel on Climate Change, 2021.

Eyring, V., Bony, S., Meehl, G. A., Senior, C. A., Stevens, B., Stouffer, R. J., and Taylor, K. E.: Overview of the Coupled Model Intercomparison Project Phase 6 (CMIP6) experimental design and organization, Geoscientific Model Development, 9, 1937–1958, https://doi.org/10.5194/gmd-9-1937-2016, 2016.

Eyring, V., N.P. Gillett, K.M. Achuta Rao, R. Barimalala, M. Barreiro Parrillo, N. Bellouin, C. Cassou, P.J. Durack, Y. Kosaka, S. McGregor, S. Min, O. Morgenstern, Y. Sun: Human Influence on the Climate System, n.d.

Fan, J., Wang, Y., Rosenfeld, D., and Liu, X.: Review of Aerosol–Cloud Interactions: Mechanisms, Significance, and Challenges, Journal of the Atmospheric Sciences, 73, 4221–4252, https://doi.org/10.1175/JAS-D-16-0037.1, 2016.

Feingold, G., Eberhard, W. L., Veron, D. E., and Previdi, M.: First measurements of the Twomey indirect effect using ground-based remote sensors, Geophysical Research Letters, 30, https://doi.org/10.1029/2002GL016633, 2003.

Flynn, L., Long, C., Wu, X., Evans, R., Beck, C. T., Petropavlovskikh, I., McConville, G., Yu, W., Zhang, Z., Niu, J., Beach, E., Hao, Y., Pan, C., Sen, B., Novicki, M., Zhou, S., and Seftor, C.: Performance of the Ozone Mapping and Profiler Suite (OMPS) products, Journal of Geophysical Research: Atmospheres, 119, 6181–6195, https://doi.org/10.1002/2013JD020467, 2014.

Forster, P., T. Storelvmo, K. Armour, W. Collins, J.-L. Dufresne, D. Frame, D.J. Lunt, T. Mauritsen, M.D. Palmer, M. Watanabe, M. Wild, H. Zhang: The Earth's Energy Budget, Climate Feedbacks, and Climate Sensitivity. In Climate Change

https://doi.org/10.5194/egusphere-2024-360
Preprint. Discussion started: 8 February 2024

2021: The Physical Science Basis. Contribution of Working Group I to the Sixth Assessment Report of the Intergovernmental Panel on Climate Change, 2021.

Gryspeerdt, E., Goren, T., Sourdeval, O., Quaas, J., Mülmenstädt, J., Dipu, S., Unglaub, C., Gettelman, A., and Christensen, M.: Constraining the aerosol influence on cloud liquid water path, Atmospheric Chemistry and Physics, 19, 5331–5347, https://doi.org/10.5194/acp-19-5331-2019, 2019.

Gryspeerdt, E., McCoy, D. T., Crosbie, E., Moore, R. H., Nott, G. J., Painemal, D., Small-Griswold, J., Sorooshian, A., and Ziemba, L.: The impact of sampling strategy on the cloud droplet number concentration estimated from satellite data, Atmos. Meas. Tech., 15, 3875–3892, https://doi.org/10.5194/amt-15-3875-2022, 2022.

Haghighatnasab, M., Kretzschmar, J., Block, K., and Quaas, J.: Impact of Holuhraun volcano aerosols on clouds in cloud-system-resolving simulations, Atmospheric Chemistry and Physics, 22, 8457–8472, https://doi.org/10.5194/acp-22-8457-2022, 2022.

Haywood, J. and Boucher, O.: Estimates of the direct and indirect radiative forcing due to tropospheric aerosols: A review, Reviews of Geophysics, 38, 513–543, https://doi.org/10.1029/1999RG000078, 2000.

Haywood, J. M., Jones, A., Clarisse, L., Bourassa, A., Barnes, J., Telford, P., Bellouin, N., Boucher, O., Agnew, P., Clerbaux, C., Coheur, P., Degenstein, D., and Braesicke, P.: Observations of the eruption of the Sarychev volcano and simulations using the HadGEM2 climate model, Journal of Geophysical Research: Atmospheres, 115, https://doi.org/10.1029/2010JD014447, 2010.

Ialongo, I., Hakkarainen, J., Kivi, R., Anttila, P., Krotkov, N. A., Yang, K., Li, C., Tukiainen, S., Hassinen, S., and Tamminen, J.: Comparison of operational satellite SO_2 products with ground-based observations in northern Finland during the Icelandic Holuhraun fissure eruption, Atmospheric Measurement Techniques, 8, 2279–2289, https://doi.org/10.5194/amt-8-2279-2015, 2015.

Ilyinskaya, E., Schmidt, A., Mather, T. A., Pope, F. D., Witham, C., Baxter, P., Jóhannsson, T., Pfeffer, M., Barsotti, S., Singh, A., Sanderson, P., Bergsson, B., McCormick Kilbride, B., Donovan, A., Peters, N., Oppenheimer, C., and Edmonds, M.: Understanding the environmental impacts of large fissure eruptions: Aerosol and gas emissions from the 2014–2015 Holuhraun eruption (Iceland), Earth and Planetary Science Letters, 472, 309–322, https://doi.org/10.1016/j.epsl.2017.05.025, 2017.

Jones, A., Roberts, D. L., and Slingo, A.: A climate model study of indirect radiative forcing by anthropogenic sulphate aerosols, Nature, 370, 450–453, https://doi.org/10.1038/370450a0, 1994.

Jordan, G., Haywood, J., Malavelle, F., Chen, Y., Peace, A., Duncan, E., Partridge, D. G., Kim, P., Watson-Parris, D., Takemura, T., Neubauer, D., Myhre, G., Skeie, R., and Laakso, A.: How well are aerosol-cloud interactions represented in climate models? Part 1: Understanding the sulphate aerosol production from the 2014-15 Holuhraun eruption, EGUsphere, 1–34, https://doi.org/10.5194/egusphere-2023-619, 2023.

Kuhlbrodt, T., Jones, C. G., Sellar, A., Storkey, D., Blockley, E., Stringer, M., Hill, R., Graham, T., Ridley, J., Blaker, A., Calvert, D., Copsey, D., Ellis, R., Hewitt, H., Hyder, P., Ineson, S., Mulcahy, J., Siahaan, A., and Walton, J.: The Low-Resolution Version of HadGEM3 GC3.1: Development and Evaluation for Global Climate, Journal of Advances in Modeling Earth Systems, 10, 2865–2888, https://doi.org/10.1029/2018MS001370, 2018.

Li, C., Krotkov, N. A., Carn, S., Zhang, Y., Spurr, R. J. D., and Joiner, J.: New-generation NASA Aura Ozone Monitoring Instrument (OMI) volcanic SO_2 dataset: algorithm description, initial results, and continuation with the Suomi-NPP Ozone Mapping and Profiler Suite (OMPS), Atmospheric Measurement Techniques, 10, 445–458, https://doi.org/10.5194/amt-10-445-2017, 2017.

https://doi.org/10.5194/egusphere-2024-360
Preprint. Discussion started: 8 February 2024

Li, C., Krotkov, N. A., Leonard, P., and Joiner, J.: OMPS/NPP PCA SO2 Total Column 1-Orbit L2 Swath 50x50km V2, https://doi.org/10.5067/MEASURES/SO2/DATA205, 2020a.

Li, C., Krotkov, N. A., Leonard, P. J. T., Carn, S., Joiner, J., Spurr, R. J. D., and Vasilkov, A.: Version 2 Ozone Monitoring Instrument SO_2 product (OMSO2 V2): new anthropogenic SO_2 vertical column density dataset, Atmospheric Measurement Techniques, 13, 6175–6191, https://doi.org/10.5194/amt-13-6175-2020, 2020b.

Malavelle, F. F., Haywood, J. M., Jones, A., Gettelman, A., Clarisse, L., Bauduin, S., Allan, R. P., Karset, I. H. H., Kristjánsson, J. E., Oreopoulos, L., Cho, N., Lee, D., Bellouin, N., Boucher, O., Grosvenor, D. P., Carslaw, K. S., Dhomse, S., Mann, G. W., Schmidt, A., Coe, H., Hartley, M. E., Dalvi, M., Hill, A. A., Johnson, B. T., Johnson, C. E., Knight, J. R., O'Connor, F. M., Partridge, D. G., Stier, P., Myhre, G., Platnick, S., Stephens, G. L., Takahashi, H., and Thordarson, T.: Strong constraints on aerosol–cloud interactions from volcanic eruptions, Nature, 546, 485–491, https://doi.org/10.1038/nature22974, 2017.

Mann, G. W., Carslaw, K. S., Spracklen, D. V., Ridley, D. A., Manktelow, P. T., Chipperfield, M. P., Pickering, S. J., and Johnson, C. E.: Description and evaluation of GLOMAP-mode: a modal global aerosol microphysics model for the UKCA composition-climate model, Geoscientific Model Development, 3, 519–551, https://doi.org/10.5194/gmd-3-519-2010, 2010.

McCoy, D. T. and Hartmann, D. L.: Observations of a substantial cloud-aerosol indirect effect during the 2014–2015 Bárðarbunga-Veiðivötn fissure eruption in Iceland, Geophysical Research Letters, 42, 10,409-10,414, https://doi.org/10.1002/2015GL067070, 2015.

McCoy, D. T., Field, P., Gordon, H., Elsaesser, G. S., and Grosvenor, D. P.: Untangling causality in midlatitude aerosol–cloud adjustments, Atmospheric Chemistry and Physics, 20, 4085–4103, https://doi.org/10.5194/acp-20-4085-2020, 2020a.

McCoy, I. L., McCoy, D. T., Wood, R., Regayre, L., Watson-Parris, D., Grosvenor, D. P., Mulcahy, J. P., Hu, Y., Bender, F. A.-M., Field, P. R., Carslaw, K. S., and Gordon, H.: The hemispheric contrast in cloud microphysical properties constrains aerosol forcing, Proceedings of the National Academy of Sciences, 117, 18998–19006, https://doi.org/10.1073/pnas.1922502117, 2020b.

Mulcahy, J. P., Johnson, C., Jones, C. G., Povey, A. C., Scott, C. E., Sellar, A., Turnock, S. T., Woodhouse, M. T., Abraham, N. L., Andrews, M. B., Bellouin, N., Browse, J., Carslaw, K. S., Dalvi, M., Folberth, G. A., Glover, M., Grosvenor, D. P., Hardacre, C., Hill, R., Johnson, B., Jones, A., Kipling, Z., Mann, G., Mollard, J., O'Connor, F. M., Palmiéri, J., Reddington, C., Rumbold, S. T., Richardson, M., Schutgens, N. A. J., Stier, P., Stringer, M., Tang, Y., Walton, J., Woodward, S., and Yool, A.: Description and evaluation of aerosol in UKESM1 and HadGEM3-GC3.1 CMIP6 historical simulations, Geoscientific Model Development, 13, 6383–6423, https://doi.org/10.5194/gmd-13-6383-2020, 2020.

NASA Worldview: https://worldview.earthdata.nasa.gov/, last access: 1 June 2023.

Peace, A. H., Carslaw, K. S., Lee, L. A., Regayre, L. A., Booth, B. B. B., Johnson, J. S., and Bernie, D.: Effect of aerosol radiative forcing uncertainty on projected exceedance year of a 1.5 °C global temperature rise, Environ. Res. Lett., 15, 0940a6, https://doi.org/10.1088/1748-9326/aba20c, 2020.

Pfeffer, M. A., Bergsson, B., Barsotti, S., Stefánsdóttir, G., Galle, B., Arellano, S., Conde, V., Donovan, A., Ilyinskaya, E., Burton, M., Aiuppa, A., Whitty, R. C. W., Simmons, I. C., Arason, Þ., Jónasdóttir, E. B., Keller, N. S., Yeo, R. F., Arngrímsson, H., Jóhannsson, Þ., Butwin, M. K., Askew, R. A., Dumont, S., Von Löwis, S., Ingvarsson, Þ., La Spina, A., Thomas, H., Prata, F., Grassa, F., Giudice, G., Stefánsson, A., Marzano, F., Montopoli, M., and Mereu, L.: Ground-Based Measurements of the 2014–2015 Holuhraun Volcanic Cloud (Iceland), Geosciences, 8, 29, https://doi.org/10.3390/geosciences8010029, 2018.

Pincus, R. and Baker, M. B.: Effect of precipitation on the albedo susceptibility of clouds in the marine boundary layer, Nature, 372, 250–252, https://doi.org/10.1038/372250a0, 1994.

Platnick, S., Meyer, K. G., King, M. D., Wind, G., Amarasinghe, N., Marchant, B., Arnold, G. T., Zhang, Z., Hubanks, P. A., Holz, R. E., Yang, P., Ridgway, W. L., and Riedi, J.: The MODIS cloud optical and microphysical products: Collection 6 updates and examples from Terra and Aqua, IEEE Trans Geosci Remote Sens, 55, 502–525, https://doi.org/10.1109/TGRS.2016.2610522, 2017.

Platnick, S., Ackerman, S., King, M., et al: MYD06_L2 MYD06_L2 MODIS/Aqua Clouds 5-Min L2 Swath 1km and 5km, https://doi.org/10.5067/MODIS/MYD06_L2.061, 2015.

Rao, S., Klimont, Z., Smith, S. J., Van Dingenen, R., Dentener, F., Bouwman, L., Riahi, K., Amann, M., Bodirsky, B. L., van Vuuren, D. P., Aleluia Reis, L., Calvin, K., Drouet, L., Fricko, O., Fujimori, S., Gernaat, D., Havlik, P., Harmsen, M., Hasegawa, T., Heyes, C., Hilaire, J., Luderer, G., Masui, T., Stehfest, E., Strefler, J., van der Sluis, S., and Tavoni, M.: Future air pollution in the Shared Socio-economic Pathways, Global Environmental Change, 42, 346–358, https://doi.org/10.1016/j.gloenvcha.2016.05.012, 2017.

Rayner, N. A., Parker, D. E., Horton, E. B., Folland, C. K., Alexander, L. V., Rowell, D. P., Kent, E. C., and Kaplan, A.: Global analyses of sea surface temperature, sea ice, and night marine air temperature since the late nineteenth century, Journal of Geophysical Research: Atmospheres, 108, https://doi.org/10.1029/2002JD002670, 2003.

Regayre, L. A., Schmale, J., Johnson, J. S., Tatzelt, C., Baccarini, A., Henning, S., Yoshioka, M., Stratmann, F., Gysel-Beer, M., Grosvenor, D. P., and Carslaw, K. S.: The value of remote marine aerosol measurements for constraining radiative forcing uncertainty, Atmospheric Chemistry and Physics, 20, 10063–10072, https://doi.org/10.5194/acp-20-10063-2020, 2020.

Reutter, P., Su, H., Trentmann, J., Simmel, M., Rose, D., Gunthe, S. S., Wernli, H., Andreae, M. O., and Pöschl, U.: Aerosol- and updraft-limited regimes of cloud droplet formation: influence of particle number, size and hygroscopicity on the activation of cloud condensation nuclei (CCN), Atmospheric Chemistry and Physics, 9, 7067–7080, https://doi.org/10.5194/acp-9-7067-2009, 2009.

Schmidt, A., Leadbetter, S., Theys, N., Carboni, E., Witham, C. S., Stevenson, J. A., Birch, C. E., Thordarson, T., Turnock, S., Barsotti, S., Delaney, L., Feng, W., Grainger, R. G., Hort, M. C., Höskuldsson, Á., Ialongo, I., Ilyinskaya, E., Jóhannsson, T., Kenny, P., Mather, T. A., Richards, N. A. D., and Shepherd, J.: Satellite detection, long-range transport, and air quality impacts of volcanic sulfur dioxide from the 2014–2015 flood lava eruption at Bárðarbunga (Iceland), Journal of Geophysical Research: Atmospheres, 120, 9739–9757, https://doi.org/10.1002/2015JD023638, 2015.

Seftor, C. J., Jaross, G., Kowitt, M., Haken, M., Li, J., and Flynn, L. E.: Postlaunch performance of the Suomi National Polar-orbiting Partnership Ozone Mapping and Profiler Suite (OMPS) nadir sensors, Journal of Geophysical Research: Atmospheres, 119, 4413–4428, https://doi.org/10.1002/2013JD020472, 2014.

Seinfeld, J. H., Bretherton, C., Carslaw, K. S., Coe, H., DeMott, P. J., Dunlea, E. J., Feingold, G., Ghan, S., Guenther, A. B., Kahn, R., Kraucunas, I., Kreidenweis, S. M., Molina, M. J., Nenes, A., Penner, J. E., Prather, K. A., Ramanathan, V., Ramaswamy, V., Rasch, P. J., Ravishankara, A. R., Rosenfeld, D., Stephens, G., and Wood, R.: Improving our fundamental understanding of the role of aerosol−cloud interactions in the climate system, Proceedings of the National Academy of Sciences, 113, 5781–5790, https://doi.org/10.1073/pnas.1514043113, 2016.

Sellar, A. A., Jones, C. G., Mulcahy, J. P., Tang, Y., Yool, A., Wiltshire, A., O'Connor, F. M., Stringer, M., Hill, R., Palmieri, J., Woodward, S., de Mora, L., Kuhlbrodt, T., Rumbold, S. T., Kelley, D. I., Ellis, R., Johnson, C. E., Walton, J., Abraham, N. L., Andrews, M. B., Andrews, T., Archibald, A. T., Berthou, S., Burke, E., Blockley, E., Carslaw, K., Dalvi, M., Edwards, J., Folberth, G. A., Gedney, N., Griffiths, P. T., Harper, A. B., Hendry, M. A., Hewitt, A. J., Johnson, B., Jones, A., Jones, C. D., Keeble, J., Liddicoat, S., Morgenstern, O., Parker, R. J., Predoi, V., Robertson, E., Siahaan, A., Smith, R. S., Swaminathan, R., Woodhouse, M. T., Zeng, G., and Zerroukat, M.: UKESM1: Description and Evaluation of the U.K. Earth System Model, Journal of Advances in Modeling Earth Systems, 11, 4513–4558, https://doi.org/10.1029/2019MS001739, 2019.

https://doi.org/10.5194/egusphere-2024-360
Preprint. Discussion started: 8 February 2024

Spracklen, D. V. and Rap, A.: Natural aerosol–climate feedbacks suppressed by anthropogenic aerosol, Geophysical Research Letters, 40, 5316–5319, https://doi.org/10.1002/2013GL057966, 2013.

Steensen, B. M., Schulz, M., Theys, N., and Fagerli, H.: A model study of the pollution effects of the first 3 months of the Holuhraun volcanic fissure: comparison with observations and air pollution effects, Atmospheric Chemistry and Physics, 16, 9745–9760, https://doi.org/10.5194/acp-16-9745-2016, 2016.

Stein, A. F., Draxler, R. R., Rolph, G. D., Stunder, B. J. B., Cohen, M. D., and Ngan, F.: NOAA's HYSPLIT Atmospheric Transport and Dispersion Modeling System, Bulletin of the American Meteorological Society, 96, 2059–2077, https://doi.org/10.1175/BAMS-D-14-00110.1, 2015.

Stevens, B. and Feingold, G.: Untangling aerosol effects on clouds and precipitation in a buffered system, Nature, 461, 607–613, https://doi.org/10.1038/nature08281, 2009.

Toll, V., Christensen, M., Gassó, S., and Bellouin, N.: Volcano and Ship Tracks Indicate Excessive Aerosol-Induced Cloud Water Increases in a Climate Model, Geophysical Research Letters, 44, 12,492-12,500, https://doi.org/10.1002/2017GL075280, 2017.

Toll, V., Christensen, M., Quaas, J., and Bellouin, N.: Weak average liquid-cloud-water response to anthropogenic aerosols, Nature, 572, 51–55, https://doi.org/10.1038/s41586-019-1423-9, 2019.

Turnock, S. T., Mann, G. W., Woodhouse, M. T., Dalvi, M., O'Connor, F. M., Carslaw, K. S., and Spracklen, D. V.: The Impact of Changes in Cloud Water pH on Aerosol Radiative Forcing, Geophysical Research Letters, 46, 4039–4048, https://doi.org/10.1029/2019GL082067, 2019.

Twigg, M. M., Ilyinskaya, E., Beccaceci, S., Green, D. C., Jones, M. R., Langford, B., Leeson, S. R., Lingard, J. J. N., Pereira, G. M., Carter, H., Poskitt, J., Richter, A., Ritchie, S., Simmons, I., Smith, R. I., Tang, Y. S., Van Dijk, N., Vincent, K., Nemitz, E., Vieno, M., and Braban, C. F.: Impacts of the 2014–2015 Holuhraun eruption on the UK atmosphere, Atmospheric Chemistry and Physics, 16, 11415–11431, https://doi.org/10.5194/acp-16-11415-2016, 2016.

Twomey, S.: Pollution and the planetary albedo, Atmospheric Environment (1967), 8, 1251–1256, https://doi.org/10.1016/0004-6981(74)90004-3, 1974.

Varon, D. J., Jacob, D. J., McKeever, J., Jervis, D., Durak, B. O. A., Xia, Y., and Huang, Y.: Quantifying methane point sources from fine-scale satellite observations of atmospheric methane plumes, Atmospheric Measurement Techniques, 11, 5673–5686, https://doi.org/10.5194/amt-11-5673-2018, 2018.

Watson-Parris, D. and Smith, C. J.: Large uncertainty in future warming due to aerosol forcing, Nat. Clim. Chang., 1–3, https://doi.org/10.1038/s41558-022-01516-0, 2022.

Wells, A. F., Jones, A., Osborne, M., Damany-Pearce, L., Partridge, D. G., and Haywood, J. M.: Including ash in UKESM1 model simulations of the Raikoke volcanic eruption reveals improved agreement with observations, Atmospheric Chemistry and Physics, 23, 3985–4007, https://doi.org/10.5194/acp-23-3985-2023, 2023.

West, R. E. L., Stier, P., Jones, A., Johnson, C. E., Mann, G. W., Bellouin, N., Partridge, D. G., and Kipling, Z.: The importance of vertical velocity variability for estimates of the indirect aerosol effects, Atmospheric Chemistry and Physics, 14, 6369–6393, https://doi.org/10.5194/acp-14-6369-2014, 2014.

Williams, K. D., Copsey, D., Blockley, E. W., Bodas-Salcedo, A., Calvert, D., Comer, R., Davis, P., Graham, T., Hewitt, H. T., Hill, R., Hyder, P., Ineson, S., Johns, T. C., Keen, A. B., Lee, R. W., Megann, A., Milton, S. F., Rae, J. G. L., Roberts, M.

https://doi.org/10.5194/egusphere-2024-360
Preprint. Discussion started: 8 February 2024

J., Scaife, A. A., Schiemann, R., Storkey, D., Thorpe, L., Watterson, I. G., Walters, D. N., West, A., Wood, R. A., Woollings, T., and Xavier, P. K.: The Met Office Global Coupled Model 3.0 and 3.1 (GC3.0 and GC3.1) Configurations, Journal of Advances in Modeling Earth Systems, 10, 357–380, https://doi.org/10.1002/2017MS001115, 2018.

Wood, R.: Stratocumulus Clouds, Monthly Weather Review, 140, 2373–2423, https://doi.org/10.1175/MWR-D-11-00121.1, 2012.

Wood, R. and Bretherton, C. S.: On the Relationship between Stratiform Low Cloud Cover and Lower-Tropospheric Stability, Journal of Climate, 19, 6425–6432, https://doi.org/10.1175/JCLI3988.1, 2006.

Zerefos, C. S., Eleftheratos, K., Kapsomenakis, J., Solomos, S., Inness, A., Balis, D., Redondas, A., Eskes, H., Allaart, M., Amiridis, V., Dahlback, A., De Bock, V., Diémoz, H., Engelmann, R., Eriksen, P., Fioletov, V., Gröbner, J., Heikkilä, A., Petropavlovskikh, I., Jarosławski, J., Josefsson, W., Karppinen, T., Köhler, U., Meleti, C., Repapis, C., Rimmer, J., Savinykh, V., Shirotov, V., Siani, A. M., Smedley, A. R. D., Stanek, M., and Stübi, R.: Detecting volcanic sulfur dioxide plumes in the Northern Hemisphere using the Brewer spectrophotometers, other networks, and satellite observations, Atmospheric Chemistry and Physics, 17, 551–574, https://doi.org/10.5194/acp-17-551-2017, 2017.

Zhou, L., Liu, Q., Liu, D., Xie, L., Qi, L., and Liu, X.: Validation of MODIS liquid water path for oceanic nonraining warm clouds: Implications on the vertical profile of cloud water content, Journal of Geophysical Research: Atmospheres, 121, 4855–4876, https://doi.org/10.1002/2015JD024499, 2016.